Journal of Analytical and Applied Pyrolysis 194 (2026) 107575

Contents lists available at ScienceDirect

Journal of Analytical and Applied Pyrolysis

journal homepage: www.elsevier.com/locate/jaap

Chemical recycling of mixed thermoplastics via pyrolysis: A comparative study of feedstock influence and reactor impact

Niklas Netsch [a], Aljoscha Tauber [a], Orhan Keskin [a], Britta Bergfeldt [a], Harald Wehner [b], Dirk Eidam [b], Salar Tavakkol [a,*], Dieter Stapf [a]

[a] Institute for Technical Chemistry, Karlsruhe Institute of Technology, Kaiserstraße 12, Karlsruhe 76131, Germany
[b] DHBW Karlsruhe, Erzbergerstraße 121, Karlsruhe 76133, Germany

ARTICLE INFO

Keywords:
Pyrolysis
Thermoplastics
Plastic waste
Chemical recycling
Stirred tank reactor
Screw reactor

ABSTRACT

Pyrolysis represents a promising solution for increasing plastic waste recycling rates in a circular economy. The thermal decomposition behavior of pure polymers is well investigated. However, the diverse composition and complex technical reactor conditions pose challenges for the pyrolysis of heterogeneous plastic waste. Therefore, this study examines the pyrolysis of virgin polymers, defined reference mixtures, and post-consumer waste in a scalable stirred tank reactor (STR) compared to an auger-type screw reactor (ASR) at pilot-scale. The results of the STR confirm that simple polymer blends of polyolefins and polystyrene degrade following the decomposition mechanisms of the pure polymer, while heteroatom-containing mixtures exhibit interaction effects. These interactions shift the products from the condensable to the gaseous fraction by up to 22 wt.%. Furthermore, product yields and compositions strongly depend on reactor design and process parameters. The gas residence time and the time-dependent polymer pyrolysis temperature are identified as the main influencing parameters. In this study, interaction effects between different polymers overlap the reactor-specific impact in complex feedstock mixtures, dominating the product yields. The condensate yield in the STR exceeds the results obtained in the ASR by 10–24 wt.% for LDPE, PP, PS, and a mixture of them. In contrast, the STR system yields only up to 6 wt.% more condensates than the ASR system for mixtures containing oxygen, nitrogen, and chlorine. The reactor type has a major impact on condensate quality. The H/C ratio, heteroatom content, and proportion of distillation cuts in the light and middle distillate range vary significantly.

1. Introduction

Growing plastic consumption and low global recycling rates require innovative technical solutions and a rethinking of plastic waste management [1]. By establishing a circular economy for plastic products, these challenges and several Sustainable Development Goals of the United Nations are being addressed [2]. Mechanical recycling is technically limited regarding the feedstock requirements and product quality. Consequently, heterogeneous waste fractions are mainly incinerated for energy recovery or landfilled [3]. Chemical recycling of plastic waste represents a promising option for the transformation to a closed-loop circular economy and for achieving higher recycling rates [4,5]. Robust thermochemical processes, such as pyrolysis or gasification, can help to fill the gap in material recycling of heterogeneous waste streams [6]. Pyrolysis offers multiple pathways to reintroduce its products into the petrochemical industry, substituting fossil-based feedstocks [7].

However, plastic pyrolysis strongly depends on the applied feedstock and the used reactor design. These dependencies often cause significant variance in experimentally determined product yields and compositions. Maqsood et al. and Soni et al. summarize numerous experimental studies on the pyrolysis of various polymers produced in different reactor technologies [8,9]. The reported yields of the generated product fractions, pyrolysis condensate, permanent gas, and solid residue, vary broadly. They conclude a yield range of 0–90, 3–90, and 0.5–78 wt.% for

Abbreviations: ABS, Acrylonitrile butadiene styrene; FID, Flame ionization detector; GC, Gas chromatograph; GRT, Gas residence time; H/C, Hydrogen to carbon ratio; HC, Hydrocarbon; HDPE, High-density polyethylene; LDPE, Low-density polyethylene; MgOx, Magnesium oxalate dihydrate; MS, Mass spectrometer; PA6, Polyamide 6; PCW, Post-consumer waste; PET, Polyethylene terephthalate; PP, Polypropylene; PS, Polystyrene; PVC, Polyvinyl chloride; STR, Stirred tank reactor; TCD, Thermal conductivity detector; VGO, Vacuum gas oil.

* Corresponding author.
E-mail address: Salar.Tavakkol@kit.edu (S. Tavakkol).

https://doi.org/10.1016/j.jaap.2025.107575
Received 29 August 2025; Received in revised form 15 December 2025; Accepted 22 December 2025
Available online 23 December 2025

these product fractions, respectively. The distinct pyrolysis mechanisms of the polymer types, consisting of countless elementary reactions, are decisive for the varying results in plastics pyrolysis. Interactions between intermediates of decomposing polymers further complicate the attribution of pyrolysis results to certain feedstock components [10,11].

Chang et al., Laghezza et al., and Faisal et al. confirm these results in their studies, whilst indicating a pronounced dependence of the resulting products on the pyrolysis temperature [12–14]. They conclude that, in general, reducing the reactor temperature leads to higher condensate yields. The formation of pyrolysis gas and solid residue, often obtained as coke, decreases accordingly. Honus et al. show that the feedstock and temperature dependency can also strongly influence the composition of the gaseous product [15]. The formation of CH_4, for example, increases as the temperature rises. Similar dependence can be observed in the pyrolysis condensate. Lopez et al. describe the shift towards aromatic products at higher reaction temperatures [7]. Moreover, reactions in the gas phase affect the pyrolysis. Secondary cracking reactions of aliphatic volatiles in the gas phase are reported for polyethylene [16]. The formation of polyaromatic components as a consequence of secondary gas phase reaction at high temperature is proven [17]. Therefore, the residence time of the volatile products at reaction temperature is another decisive factor influencing yields and composition. Overall, as the residence time of volatile products increases, secondary reactions such as secondary cracking, isomerization reactions, or aromatics and coke formation intensify similarly to rising pyrolysis temperatures [8,18].

Differences in the heat and mass transfer of technical pyrolysis systems often lead to variations of process parameters with insufficient or no experimental possibilities for detection and control [18]. For example, Dai et al. point out that even under seemingly isothermal reactor temperature, the polymers entering the reactor undergo an undefined heating process [18]. Depending on the heating, partial conversion by pyrolysis reactions occurs until the isothermal reactor temperature is reached. Therefore, the time-related temperature profile of the decomposing polymer can deviate considerably from the target pyrolysis temperature of the reactor. Inhomogeneous temperature distributions resulting from endothermic processes and heat transfer limitations are present in more complex technical reactor systems. The temperature gradients additionally enhance temperature deviations. Product backmixing in the polymer melt or within the gas phase, together with interfacial processes such as product evaporation, also prove challenges in characterizing and recording these effects. In this context, Hassibi et al. use the evaporation properties of the products to significantly influence the product yield and distribution using a reflux system while maintaining the constant feedstock and reactor temperature [19,20]. This multitude of parallel effects leads to a deficient database that complicates system evaluations [21], plant construction [14], or reactor upscaling [22] in the pyrolysis of plastic waste.

This study presents a comprehensive comparison of two common reactor types for different thermoplastic feedstocks. In preliminary tests, the STR and ASR systems are characterized in detail using analogous methods. This enables a technical comparison of fundamentally different reactor types under realistic, non-ideal conditions: a perfectly stirred reactor and a plug flow reactor. Reactor-dependent differences in the pyrolysis behavior are elucidated based on product yields and product composition. The reactor differences are attributed to specific design and operating characteristics. Defined pure thermoplastics, their mixtures, and a representative post-consumer waste (PCW) are investigated to reveal the feedstock influence. Calculations based on a linear superposition approach are performed for determining theoretical product yields and product compositions. The calculations allow for the identification of feedstock-specific interactions [11].

This study contributes to understanding the feedstock dependency of mixed thermoplastics pyrolysis and the importance of the reactor design and operation. The comparison highlights technical benefits and limitations for both reactor types. Furthermore, this work provides detailed data for process optimization and comparative process evaluation in the chemical recycling of plastics via thermal pyrolysis.

2. Materials and methods

2.1. Feedstocks

Low-density polyethylene (LDPE), polypropylene (PP), polystyrene (PS), acrylonitrile butadiene styrene copolymer (ABS), polyethylene terephthalate (PET), polyamide 6 (PA6), and polyvinyl chloride (PVC) were used in the pyrolysis experiments. Apart from PVC, the polymers were additive-free primary granules. This prevented the influence of additives, such as flame retardants, stabilizers, plasticizers, or fillers, focusing on the impact of polymers on the pyrolysis result. All thermoplastics, except for PET, were pyrolyzed as pure polymers to enable the deduction of results for mixtures from individual components. In addition, three different reference mixtures of these thermoplastics and a PCW, were pyrolyzed. PET was not pyrolyzed as a pure polymer, as the products caused rapid clogging of the reactor's exhaust piping and the condensers. Thus, PET was only used in the reference mixtures. The elemental analysis of the polymers and mixtures, as well as their moisture, ash, and polymer content, are listed in Table 1. The reference mixtures are referred to as Mix A, Mix B, and Mix C in the following. Mix A consists of 40 wt.% LDPE, 30 wt.% PP, and 30 wt.% PS. Mix B represents a less contaminated polyolefin-rich waste fraction, while Mix C is supposed to reflect a highly contaminated waste fraction. Compared to Mix B, it exhibits a higher proportion of nitrogen-, oxygen-, and chlorine-containing polymers, while reducing the polyolefin content. The PCW contained real plastic products that presumably incorporated few impurities and additives. The examined PCW originated from the same sample fraction as reported by Netsch et al. [23]. However, the PCW was additionally extruded for smooth feedstock dosing in the STR. The extrusion was performed in a single screw extruder type HAAKE PolyLab Rheomex OS (Thermo Fisher Scientific) at 200 °C. The nozzle temperature was set slightly higher at 225 °C. The mild temperature settings prevented feedstock alteration during the pre-treatment step, while ensuring form-stable extrudates with diameters ranging from 2 to 4 mm.

Magnesium oxalate dihydrate (MgOx) was used to validate the method of determining product fraction yields and deducting mass balances. MgOx features a defined two-stage decomposition mechanism [24]. This mechanism follows reaction Eq. R1 and reaction Eq. R2. Assuming complete decomposition, the product yields can be calculated from the reaction equations [24].

Table 1
Elemental Analysis of the pure polymers, reference mixtures, and the PCW [23].

Feedstock	Elemental composition in wt.%						
	C	H	N	Cl	Moisture	Ash	O[A]
LDPE	85.8	14.2	< 0.2	0.0	< 0.01	< 0.01	0.0
PP	85.8	14.2	< 0.2	0.0	< 0.01	< 0.01	0.0
PS	92.0	8.0	< 0.2	0.0	< 0.01	< 0.01	0.0
ABS	86.2	8.0	5.5	0.0	0.3	< 0.01	0.0
PET	63.3	4.4	< 0.2	0.0	0.2	< 0.01	32.1
PA6	63.6	9.8	12.6	0.0	1.2	< 0.01	12.7
PVC	36.2	4.9	< 0.2	47.9	0.2	10.6	0.2
Mix A[1,B]	87.6	12.4	< 0.2	0.0	0.0	0.0	0.0
Mix B[2,B]	83.5	13.4	0.3	1.0	0.0	0.2	1.6
Mix C[3,B]	80.6	11.6	0.9	2.4	0.1	0.5	3.9
PCW[4,B]	80.0	12.3	0.8	1.4	0.0	2.2	3.3

[1] contains 40 % LDPE, 30 % PP, 30 % PS.
[2] contains 70 % LDPE, 20 % PP, 4 % PET, 2 % PS, 2 % PA6, 2 % PVC.
[3] contains 50 % LDPE, 15 % PP, 10 % PET, 10 % PS, 5 % ABS, 5 % PA6, 5 % PVC.
[4] contains 29.4 % LDPE, 25.1 % PP, 17.1 % HDPE, 10.1 % PET, 6.3 % PA6, 4.2 % PS, 4.0 % PVC, 3.8 % ABS.
[A] calculated as the difference to 100 wt%.
[B] calculated from the proportion of individual polymers in the mixture

$$Mg(C_2O_4) \bullet 2H_2O \rightarrow Mg(C_2O_4) + 2H_2O \quad \text{(R1)}$$

$$Mg(C_2O_4) \rightarrow MgO + CO_2 + CO \quad \text{(R2)}$$

2.2. Stirred tank reactor

The experiments were conducted in a scalable STR system. Fig. 1 schematically depicts this pyrolysis system. The detailed piping and instrumentation diagram and engineering drawings of reactor parts are provided in the supplementary information (S1). The cylindrical reactor featured a total volume of about 2.7 L. Two electrical heating sleeves with a power of 1.25 kW supplied the energy for the endothermic process by heating the outer reactor wall. Two thermocouples were arranged on the outer reactor wall to regulate the temperature of the reactor heating system, thereby ensuring a constant reactor wall temperature. Flange accesses were located on top of the reactor vessel. They were used for polymer addition, the installation of a thermocouple monitoring the inner reactor temperature, and a gas exhaust towards the condensation unit. The locations of thermocouples employed in this system can also be found in the supplementary information (S1). The reactor was equipped with a customized Paravisc-type impeller (Ekato GmbH). The stirrer was driven by an electric motor with a maximum torque of 12 Nm. The agitator shaft was flushed below the shaft seal via a nitrogen inlet. The polymer was added into a vertical fall neck equipped with a lock of two ball valves. A storage container was located above the second valve, and another nitrogen inlet was below the valve lock. It served as the primary flush gas inlet. Like the nitrogen inlet at the shaft flushing, a mass flow controller enabled a defined addition of Nitrogen. Together with the flush gas, product gases and volatile substances left the reactor through the exhaust pipe into the first condensation stage. This stage consisted of two vertically arranged double-tube heat exchangers of each 1.5 m length. At the bottom of the condensation stage, condensing products were collected in a glass flask. A second condensation stage of the same design followed, but concluded with an electrostatic precipitator. The condensing products in this stage were captured in an analogous arrangement to the first stage. The temperatures in both stages could be flexibly adjusted in the range of −25–100 °C using circulation thermostats. Demineralized water and a water-glycol mixture were used as heating and cooling media. Online gas sensors analyzed the remaining permanent gas before they were transferred to the flare. Additionally, the permanent gas was sampled via gas bags for offline analyses in a gas chromatograph (GC).

The reactor was inerted with nitrogen before the experimental start. The feedstock was loaded into the storage container, flushed by nitrogen, and then placed on the upper part of the closed valve lock. The connection between the reactor and the first condensation stage was heated to a temperature of 380 °C with trace heaters to prevent blocking caused by condensing products. The condensation stages were heated and cooled to 60 and -5 °C, respectively. The connection between the two condensation stages and the section between both heat exchangers of the first condensation stage were heated to 60 °C with trace heaters. The main purge gas flow was set to 2 L_{NTP}/min during operation (volume flow referenced to normal temperature and pressure). This setting enabled the defined transport of generated product gases through the condensation stages into the gas analysis. The purge gas flow of 0.3 L_{NTP}/min ensured that no volatile products entered the agitator shaft sealing. The nitrogen flow at the electrostatic precipitator was 1 L_{NTP}/min in experimental operation.

Ideally, the STR offers uniform polymer distribution. However, the semi-continuous feeding method with punctual injection hindered this. Time- and location-dependent fluctuations are expected but can be minimized by methodological adaptations and selecting optimal stirring parameters. At the start of the experiment, the reactor was filled with 2 kg of quartz sand. Applying quartz sand as a homogenizing agent accelerated the mixing of the highly viscous thermoplastic melt and sticky intermediates, which formed upon polymer addition [14]. Mixing effects dependent on the sand to polymer ratio and the selection of the optimal stirrer geometry were investigated in preliminary cold model tests. Sand, polymer, and silicon oil were used to reflect sand-polymer mixtures in the pyrolysis reactor. By applying the silicon oil with a dynamic viscosity of 97 and 970 Pa•s, the polymer melt could be simulated in the cold model operated at room temperature. The employed quartz sand featured a particle size of 1–4 mm. Before the experiment started, the stirrer speed was set to 50 rpm. Optimal stirring speed was verified visually using an endoscope camera in the STR system at ambient temperature. As reported by Abbas-Abadi et al., increasing the stirrer speed to 50 rpm led to more extensive mixing [26]. Higher speed further improved the mixing, but also caused intensive abrasion of the sand particles, leading to disadvantageous dust formation. In all experiments, the sand-filled reactor was preheated to a reactor wall temperature of

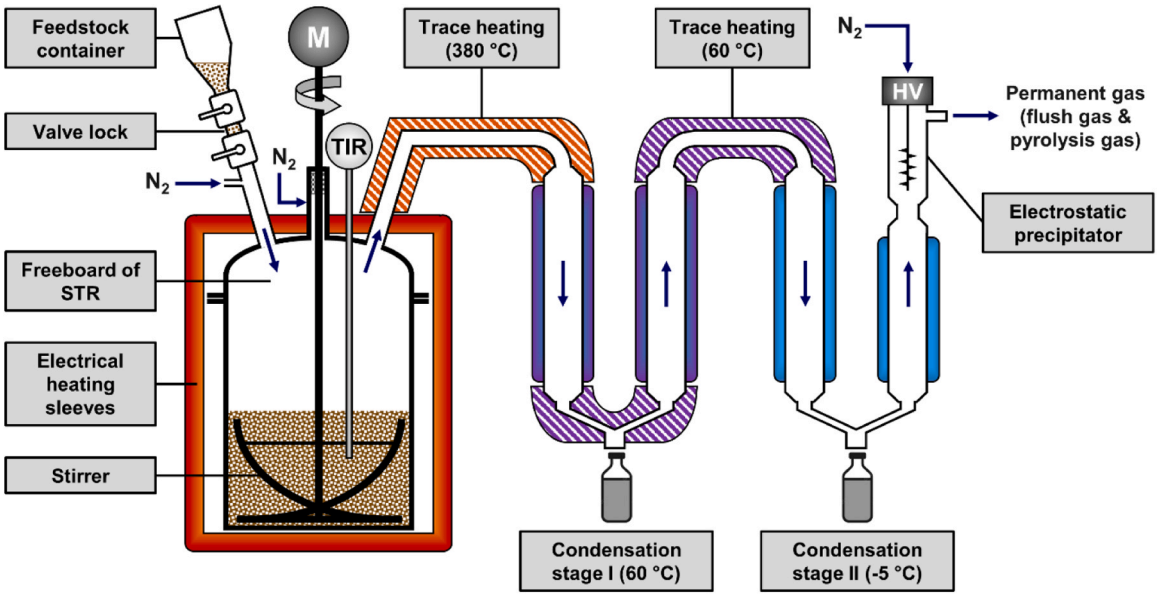

Fig. 1. Schematic illustration of the STR setup consisting of a feeding system, an externally heated sand stirred reactor with a thermocouple recording the internal reactor temperature, and a two-stage condensation system including an electrical precipitator.

500 °C before adding the feedstock. The temperature of 500 °C was chosen to meet optimal conditions of high condensate yields while minimizing the formation of waxes and coke [17,25].

Once the reactor temperature stabilized, the feedstock was introduced into the hot reactor in small batches at five-minute intervals by adjusting the position of the two ball valves. Premixing of Mix A, Mix B, and Mix C in the feedstock container ensured a constant feedstock composition in each feeding cycle. A total quantity of 250 g was added per experiment. Depending on the feedstock's density, between 23 (PCW) and 37 g (PVC) was introduced per feed cycle. This semi-continuous mode of operation was intended to ensure defined isothermal conditions and consistent product formation. The electrostatic precipitator removed condensate droplets from the gas flow at 10 kV. While simultaneously avoiding product build-up at cold spots, condensable products were separated from the permanent gas as effectively as possible in this setup. Gas samples for offline analyses were taken at specific times, usually after the fifth and eighth feeding cycle (21 and 36 min). The experimental settings were maintained for at least 1.5 h following the last material input. The delay time ensured a complete conversion, sufficient time for the product separation in the condensers, and the purging of all gases in the pyrolysis system [17]. After the experiment, the mixture of sand and the remaining solid pyrolysis product, the so-called solid residue, was weighed. The condensate flasks were also weighed before and after the test run.

2.3. Auger-type screw reactor

The ASR system operates on a pilot scale. Thus, it has significantly larger dimensions, with a screw length of 2.5 m and a freeboard volume of about 80 L. The system contains a feedstock dosing section, the screw reactor with an integrated hot gas filtration system, a two-stage condensation system, and a gas analysis section. A schematic overview of the ASR reactor is displayed in Fig. 2.

For comparison, the pyrolysis experiments were conducted at 500 °C reactor wall temperature. As with the STR system, the reactor was heated and flushed by nitrogen before feedstock addition. The pure polymers or polymer mixtures were introduced with a feeding rate of 1 kg/h. Also, quartz sand is used. The mass ratio of sand to polymer accounted for 4:1. The flush gas flow rate was set to 12 L_{NTP}/min. The polymer-sand mixture was fed continuously into the screw reactor, where it was forced through. During this transport in the reactor, the polymers heated up, melted, and pyrolyzed. The solid residence time was set to 45 min to ensure complete conversion. During transport through the reactor, the polymer-sand mixture experienced minimal mixing compared to the STR system, as the screw rotation speed of about 1 rpm is low. Solid residues remained in the reactor and were moved to a storage container together with the sand. The pyrolysis gas, containing permanent gases and volatiles, evolved into the freeboard, passed the hot gas filtration system, and entered the two-stage condensation system. The condensation system operated at 60 and 0 °C. Trace heaters prevent the uncontrolled condensation of volatiles before they enter the condensation unit. The condensation system is technically similar to the STR in terms of dimensions and process parameters. Each condensation stage included an electrostatic precipitator at the outlet. The composition and properties of the permanent gas are analyzed online. More details on the reactor design are described elsewhere [23]. Reliable reactor comparisons are possible as a result of the similarity between the STR and ASR peripheries, identical analysis methods, and the application of the same feedstocks.

2.4. Reactor characteristics

The reactor design and the operational settings have a distinct influence on various pyrolysis process parameters. Consequently, the extensive characterization of the STR and ASR system was essential for comparing corresponding measurements. Special focus was set on the residence time of products in the reaction zone of the pyrolysis system and the time-dependent temperature distribution of the polymer during pyrolysis.

2.4.1. Gas residence time

The residence time of volatile products and permanent gases can significantly influence the yields and product composition, as sufficient residence time allows for isomerization reactions, aromatics formation, or secondary cracking of the primary pyrolysis products [17,26]. It is defined as the time required from the formation of these primary pyrolysis products in the reactor until the removal of condensables from the permanent gas in the condensation unit. In the following, it is further referred to as gas residence time (GRT). Two consecutive parts contribute to the GRT. Firstly, it includes the gas transport within the sand-melt system into the freeboard of the reactor. This mass transfer is challenging to investigate experimentally. Secondly, the mass transfer from the gas phase in the reactor freeboard to the condensation system inlet contributes to the GRT. This GRT is referred to as GRT in the hot reaction zone in the following. The GRT in the condensation system is also estimated, as it can impact the efficiency of the gas-liquid

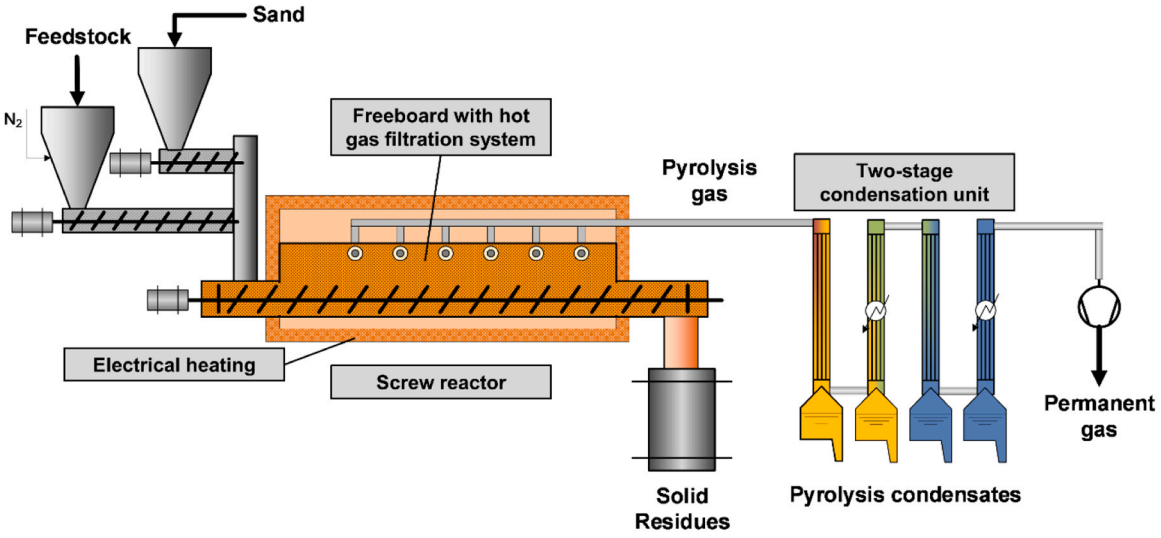

Fig. 2. Schematic illustration of the ASR system consisting of a feedstock and a sand dosing system, a screw reactor with integrated hot gas filtration, and a two-stage condensation system.

separation. This parameter covers the time required for the permanent gas to flow from the condensation inlet to the outlet of the electrical precipitator.

To estimate the GRT, CO_2 and N_2 were injected alternately into the sand-filled reactor until complete atmosphere replacement. The GRT estimation was conducted while no plastic was processed. Different insertion locations of the gases led to their detection with varying time delays. The inserts were located at the access flanges of the upper STR part, as well as directly before the first and after the last condenser. The density variations were recorded by a sensor to quantify the time delay. With the time delay varying between 5 s and 4 min, depending on the insert location, the GRT in the hot reaction zone can be ascertained. Because of back-mixing effects and inhomogeneous flow conditions, a residence time distribution evolved. The minimum GRT and its width characterize this GRT distribution. The minimum GRT represents the shortest period the gas molecules need from the reactor to the inlet of the condensation stage. The wider the distribution, the more pronounced the presence of back-mixing effects. With both characteristic parameters, the pyrolysis processes could be compared. These parameters depended mainly on the selected amount of flush gas and the reactor geometry. Also, the volume change of gases caused by different temperatures influenced the gas residence time. It was therefore determined for both reactor systems at operating conditions (500 °C) and at room temperature. The results of the gas residence time determination of the STR are listed in Table 2 in comparison with analogous measurements in the ASR described by Netsch et al. [23].

The minimum GRT at 2.3 L_{NTP}/min flush gas flow is approximately 17–20 s in the STR at both temperatures. The higher gas velocities in the hot reactor led to fast flushing, causing a narrower distribution of about 84 s. As a result of the higher reactor temperature and thus a temperature-induced increase in the flush gas volume flow in the reactor, the GRT width decreases significantly. In the STR, comparatively low freeboard volumes result in rapid flushing of the gas phase, with relatively little back-mixing. In comparison, the minimum GRT and the GRT distribution width are significantly higher in the ASR, with about 41 and 307 s, respectively. Therefore, secondary reactions of volatiles and gas molecules are expected to be more pronounced in the ASR pyrolysis system. The polymer-sand mixture is intensively mixed in the STR, and a large surface area of the polymer-sand bed is available in the ASR system. Therefore, the contribution of the mass transport from the sand-melt system to the freeboard is assumed to be comparatively negligible. Both reactor systems feature a condensation system of similar design. The minimum GRT accounts for about 1–2 min in both reactors. Comparable GRT distribution widths of about 100–120 s are estimated for the condensation systems, reflecting similar backmixing. The GRTs are therefore comparable, which implies a negligible impact on the efficiency of separating condensable and non-condensable products. This enables the comparison of the reactors for product yields and product compositions.

2.4.2. Temperature distribution

The temperature profile is an important characteristic of pyrolysis reactors. It is linked to temperature gradients and thus the feedstock heating. Besides the polymer-specific material properties (e.g., thermal conductivity, heat capacity, pyrolysis energy demand, particle size, and particle density), the temperature distribution dominantly affects product yields through primary polymer decomposition and secondary reaction kinetics. Depending on the reaction speed and heating rate, the temperature of the pyrolyzing polymer can be significantly lower than the reactor set temperature. With the thermocouple in contact with the feedstock-sand mixture inside the STR system, the temperature of the polymeric feedstock was recorded over time. This allowed for comparison with the reactor wall temperature. Fig. 3 depicts this comparison in experiments with LDPE, PS, PVC, and PCW at a reactor wall temperature of 500°C in the STR system. An average polymer temperature is also depicted as a dashed line. This temperature specifies the time-related average of the polymer temperature during its reaction, which can already start during the heating phase. Averaging is performed over the course of all 5 min feeding cycles. The semi-continuous dosing method with the feeding cycles is clearly visible in all curves. Because of varying polymer densities, the total feedstock mass of 250 g resulted in between seven and eleven dosing intervals for PVC and PCW, respectively. After each interval, the temperature of the polymer-sand bed in the hot reaction zone declined because of endothermic processes such as polymer heating, melt transition, and pyrolysis reaction. As this process continued, further energy was introduced through the heating sleeves, causing the temperature of the polymer-sand mixture to rise again. Therefore, the fluctuating polymer temperature varied on average by approximately 30–50 °C below the reactor wall temperature, depending on the feedstock. The maximal fluctuation accounted for LDPE up to 96 °C. In contrast, the reactor wall only experienced minor temperature fluctuations of 5 °C in maximum. In general, a rapid temperature acclimatization of the polymers is seen after dosing. The fast heating of the polymers is caused by the fast homogenization of the feedstock with the hot sand mixture in less than 10 s. Compared to PVC, LDPE, and PS represent polymers exhibiting higher pyrolysis energy demand. Consequently, PVC reveals the lowest deviation between internal temperature and wall temperature, LDPE and PS the highest. The PCW curve shows a progression between the previously mentioned examples.

Due to the complexity of the moving screw trajectory in the sand-polymer mixture, temperature monitoring within the polymer-sand bed was technically not feasible in the ASR system. Nevertheless, lower heating rates of the polymers can be assumed, as the polymer did not undergo fast and extensive mixing with hot sand particles as in the STR system. Several thermocouples located directly under the feedstock at the reactor wall allowed spatial temperature differences to be monitored during steady-state operation. The temperature measured by a thermocouple located 28 cm from the reactor inlet fluctuated by a maximum of 10 °C, independently of the feedstock composition. Standard deviations of 5.4, 2.8, 1.4, and 0.3 °C are recorded at reactor lengths of 28, 83, 139, and 193 cm, respectively. They emphasize that the majority of endothermic processes occur at the front of the reactor because of continuous feedstock transport from the inlet to the outlet. On the contrary, the continuous feeding method also leads to a more constant feedstock supply, which results in smoother reactor heating and less time-dependent fluctuations. Along with the significantly larger dimensions of the reactor, a higher polymer temperature is therefore expected at the end of the heating process than was observed with the STR. However, with a presumably slower heating rate in the ASR, parts of the polymer will have reacted before this end temperature is reached.

Table 2
Characteristic GRT distribution parameters of the investigated STR and ASR systems used for investigation.

Reactor	STR		ASR
Reactor temperature in °C	ambient	500	500
Minimum GRT in the hot reaction zone in s	17 ± 4	20 ± 3	41 ± 13
Width of GRT in the hot reaction zone in s	150 ± 13	84 ± 23	307 ± 21

2.5. Analytical methods

The composition of the pyrolysis gas was determined by analyzing the gas bag samples with an advanced GC system. The system is based on an Agilent 8890 GC, which was customized with an additional isothermal oven by Teckso GmbH. Three detectors (thermal conductivity detector (TCD), flame ionization detector (FID), and Agilent 5977 C mass spectrometer (MS)) enabled the simultaneous identification and quantification of multiple gases. Details on the setup and the method parameters are summarized in the supplementary information

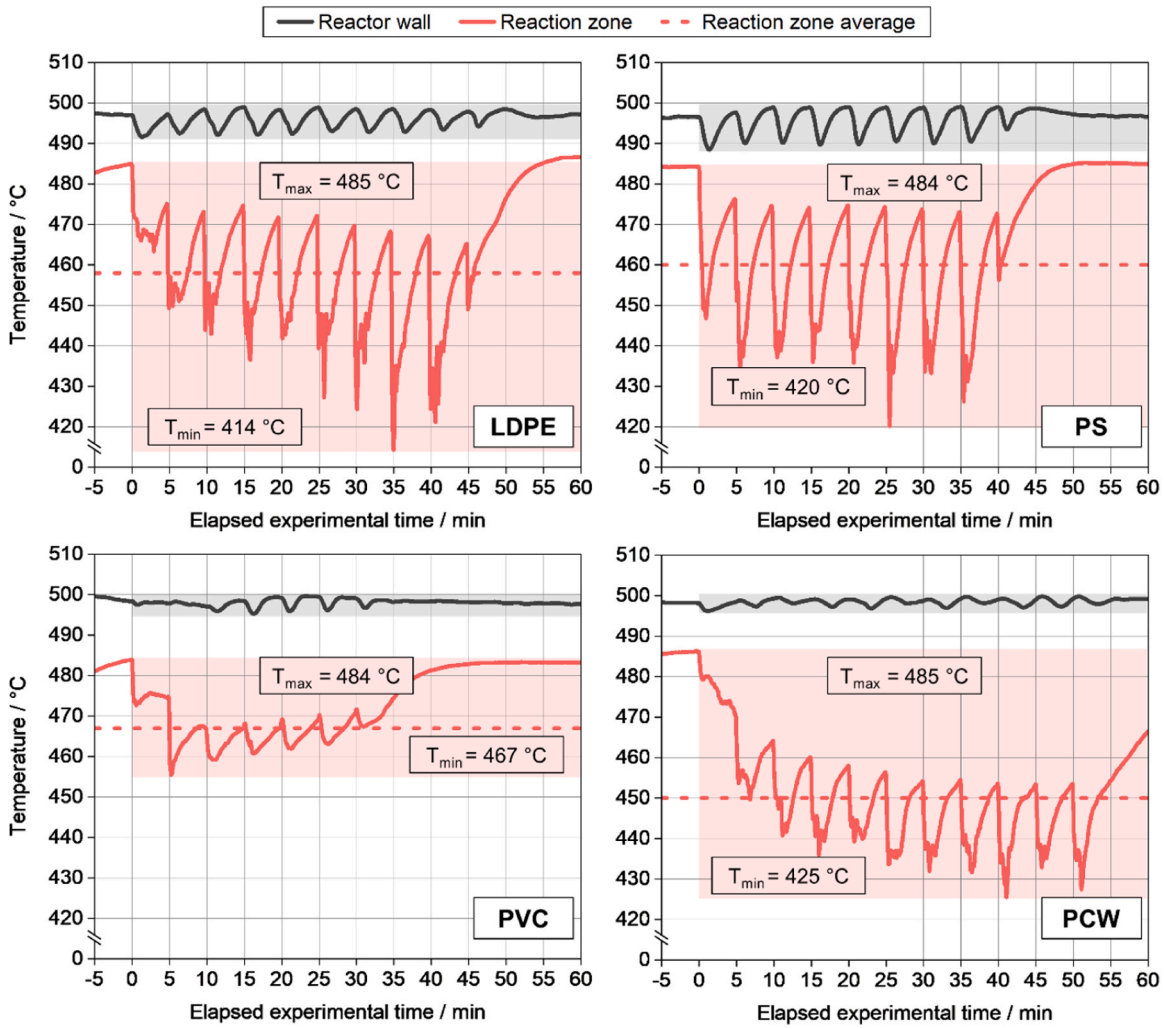

Fig. 3. Time-dependent temperature profile of the STR reactor wall and the internal temperature of the polymer-sand mixture for experiments with LDPE, PS, PVC, and PCW at 500 °C reactor wall temperature.

(S2). The TCD allowed for analyzing N_2, O_2, and main product gases such as CO_2, CO, and CH_4. The use of helium as the carrier gas prevented the quantification of H_2. The MS enabled the identification of aliphatic and aromatic hydrocarbons (HC) ranging from C_2 to C_{10}, along with gaseous HCs comprising oxygen, nitrogen, and chlorine. These gases were quantified based on the FID signal. The sample was withdrawn from gas bags storing pyrolysis gas generated at the pyrolysis systems. Further details on the setup and mode of operation, such as the valve switching during the analytical procedure, are described in detail by Zeller et al. [27]. For quantification, the main gas species and expected trace gases were calibrated at least by a 3-point calibration, employing a linear calibration curve.

The condensate characterization required a variety of complementary analyses [28]. The elemental analysis for carbon, hydrogen, and nitrogen was carried out with a LECO Truspec CHN Micro elemental analyzer according to DIN EN 15104. An analyzer consisting of an AQF-2100 combustion system combined with an Aquion ion chromatograph (a1-environsciences GmbH and Thermo Fisher Scientific GmbH) enabled the determination of the chlorine content. The water content in the condensates was measured based on DIN 51777 using Karl Fischer titration with a 870KF Titrino (Methrom). The calorific value of the condensates was determined using a C5000 calorimeter (IKA GmbH & Co. KG) according to DIN 51900. Simulated distillation performed under ASTM D 7169:2020 provided information on the product distribution of the condensates based on the boiling curve. In addition, two-dimensional GC was performed to identify and quantify the main components of the condensate. The oils were analyzed by three parallel detectors: FID, MS, and a nitrogen-chemiluminescence detector. Details on the columns and parameters relevant to GC operation are described in the supplementary information (S2). The analysis system allowed the distinction between different product groups. Aliphatics, monoaromatics, indenes, biphenyls, higher aromatic compounds, and heteroatom-containing HCs were distinguished. Further information on the development of this two-dimensional GC method and the data processing can be found elsewhere [28].

2.6. Calculations

The mass balance distinguished between the evolving product fractions: solid residue, condensate, and pyrolysis gas. The feedstock-related yield of the condensate y_{Cond} was determined by weighing the resulting condensate mass in the bottles of condensation stage 1 $m_{Cond,1}$ and stage 2 $m_{Cond,2}$ before and after the experiment according to formula 1.

$$y_{Cond} = \frac{(m_{Cond,1} - m_{Cond,1,Tare}) + (m_{Cond,2} - m_{Cond,2,Tare})}{m_{Feedstock}} \quad (1)$$

The yield of solid residue y_{Res} was calculated similarly using formula 2. Here, the weighed mass of sand and solid residue $m_{Sand+Res}$ after the test minus the initially added mass of quartz sand m_{Sand} was considered.

$$y_{Res} = \frac{(m_{Sand+Res} - m_{Sand})}{m_{Feedstock}} \quad (2)$$

By incinerating the remaining solid content in the reactor, the proportion of combustibles was determined. This value approximately corresponds to the content of coke y_{Coke} formed during pyrolysis. The coke yield was calculated from the mass before incineration $m_{Sand+Res,raw}$ and after incineration $m_{Sand+Res,incinerated}$ according to formula 3.

$$y_{Coke} = \frac{(m_{Sand+Res,raw} - m_{Sand+Res,incinerated})}{m_{Feedstock}} \quad (3)$$

The yield of pyrolysis gas $y_{Pyr.gas}$ was quantified following formula 4. This calculation required the total gas volume flow $\dot{V}_{Gas}$ and the gas density ρ_{Gas} to be integrated over the experimental phase. In addition, the purge gas mass $m_{Flushgas}$ had to be considered.

$$y_{Pyr.gas} = \frac{\left(\int_{Start}^{End} \dot{V}_{Gas}\, \rho_{Gas}\right) - m_{Flush\ gas}}{m_{Feedstock}} \quad (4)$$

According to Formula 5, the purge gas volume was calculated from the standard density of nitrogen $\rho_{Flushgas}$ and the purge gas volume flow $\dot{V}_{Flushgas}$ set at the mass flow controllers.

$$m_{Flushgas} = \dot{V}_{Flushgas}\, \rho_{Flushgas} \quad (5)$$

The pyrolysis gas composition was determined by integrating the individual peak areas of gases identified in the GC analysis. The calculation was based on the procedure described by Zeller et al. [27]. The concentration of each gas species c_i was calculated using its determined peak area A_i and the gas-specific response factor R_i as shown in formula 6 [27].

$$c_i = \frac{A_i}{R_i} \quad (6)$$

From the molar mass of the gas species M_i and the standard molar gas volumeM_{Gas}, the volume fraction of the gas species in the product gas v_i was calculable according to formula 7 [27].

$$v_i = c_i \frac{M_{Gas}}{M_i} \quad (7)$$

The comprehensive gas characterization, with over 99 vol.% of determined compounds in all experiments (except for PVC), allowed the overall balance of the gas phase to be nearly closed. Therefore, the volume fractions were normalized to 100 vol.% except for the pure PVC pyrolysis gas. Quantification of HCl was not possible with the GC method. However, relevant quantities of HCl could be identified by MS in the PVC tests. Within this particular sample, HCl was assumed to account for the balance gap. HCl is therefore included in the normalization procedure as the difference from a completely closed balance. The pyrolysis gas density $\rho_{Pyr.gas}$ was calculated using the normalized volume fractions and the density of the gases ρ_i relying on the ideal gas law as defined in formula 8 [27]. This was required to determine the normalized mass fractions of the gases x_i for the pyrolysis gas composition according to formula 9 [27].

$$\rho_{Pyr.gas} = \sum_i (v_i\, \rho_i) \quad (8)$$

$$x_i = v_i \frac{\rho_i}{\rho_{Pyr.gas}} \quad (9)$$

In this study, a model approach was used to calculate product yields and composition for the pyrolysis of plastic mixtures. It was based on the linear combination of experimental values of the individual polymer components and has already been successfully applied for calculations of product yields [29], reaction kinetics [11], or the energy demand [23] in plastic pyrolysis. The theoretical values represent a reference value under an idealized assumption. The reaction mechanisms of the polymers in the mixture are assumed to occur independently of each other, neglecting polymer-type-dependent interactions. This approach is referred to as the superposition assumption. The calculated yields y_{theo} for the product fraction were estimated from the proportions w_j of the pure substances j in the mixture and the respective product fractions during their pyrolysis y_j according to formula 10 [29].

$$y_{theo} = \sum_j \left(w_j\, y_j\right) \quad (10)$$

Model calculations of the composition of gases and condensates were carried out analogously. The content of a component $x_{i,theo}$ was calculated from the weight fraction in the pure polymer $x_{i,j}$, considering the polymer proportion in the mixture and the normalized polymer-related yield of this product fraction as defined in formula 11 [29].

$$x_{i,theo} = \sum_j x_{i,j} \bullet \left(\frac{w_j \bullet y_j}{\sum_j w_j \bullet y_J}\right) \quad (11)$$

3. Results

3.1. Stirred tank reactor

The experimental results for the pyrolysis of different feedstocks in the STR system include the yields of the product fractions and their respective chemical compositions. The product analyses focus on organic products, meaning pyrolysis oil and pyrolysis gas.

3.1.1. Product fraction yields

Experiments with MgOx were conducted for preliminary validation of the STR reactor setup. The results are averaged from three different experiments. The yields for pyrolysis gas, condensable products, and solid residue amount to 47.5, 22.3, and 29.1 wt.%, respectively. The statistical fluctuations of a maximum of 0.9 wt.% indicate excellent reproducibility. The mass balance closes up to 0.8 wt.%. Based on the stoichiometry of a complete thermal decomposition, the expected reaction products of MgOx account for 48.5 wt.% of gaseous products (carbon dioxide and carbon monoxide), 24.3 wt.% of water, and 27.2 wt.% of solid residue in the form of magnesium oxide. The experimental yields are consistent with the theoretically expected yields. The gas density sensor with its oscillating membrane proves to be unsuitable for tests with polyolefins and PVC. Therefore, no reliable density measurements are available for these tests. Consequently, the gas yield is assumed to represent the difference from a closed mass balance.

Fig. 4 shows an overview of the product yields obtained in pyrolysis experiments at 500 °C. The comprehensive data set, including all values, is listed in the supplementary information (S3). Pyrolyzing the polyolefins, LDPE and PP, mainly condensable products with 72.3 and 71.3 wt.% are formed. For PS and ABS, 98.5 and 91.2 wt.% of condensate are obtained, respectively, and almost no solid residue is formed. In the ABS experiments, 5.4 wt.% of pyrolysis gas is yielded. In these experiments, the balance loss is very low at 0.1 and 0.3 wt.%. With 76.1 wt.% PA6 pyrolysis mostly yields condensable products. The proportion of gas accounts for 20.4 wt.%. Both heteroatom-containing plastics, ABS and PA6, form solid residue with 3.5 wt.%. This solid residue is mainly comprised of coke. In the case of PVC, more pyrolysis gas with a yield of 60.2 wt.% is produced. Only a minor yield of condensable products is obtained. With 28.9 wt.%, a significant amount of solid residue remains in the reactor. This solid residue can be further specified by incineration. This residue is comprised by about 17 wt.% of coke and 12 wt.% of incombustibles.

The feedstocks Mix A, Mix B, Mix C, and PCW consist of over 70 wt.% of polyolefins. The additional proportion of PS in Mix A increases the condensate yield to 79.3 wt.%. However, this test also shows a higher experimental uncertainty of approximately 7.2 wt.% compared to the

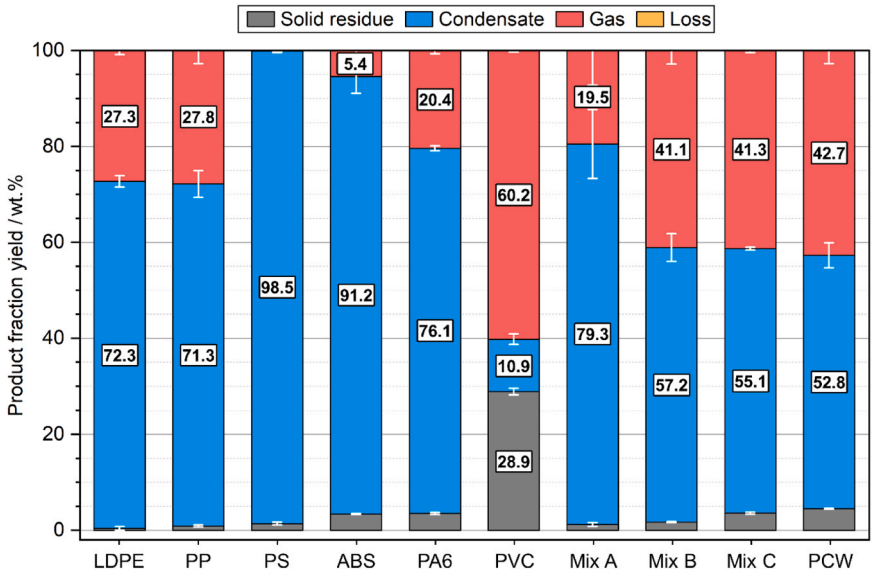

Fig. 4. Mass yields of the pyrolysis experiments with thermoplastics at 500 °C reactor wall temperature in the STR system.

other experiments. The gas yield accounts for 19.5 wt.%. Despite the different proportions of polyolefins, similar results are generated for the heteroatom-containing polymer blends Mix B and Mix C. The condensate yield amounts to 57.1 and 55.1 wt.%, respectively. Mix C generates slightly more solid residue (3.6 wt.%) than Mix B (1.7 wt.%), reflecting the higher PVC and PET content. The PCW exhibits a similar polymer composition to Mix C. The solid residue yield is slightly increased.

3.1.2. *Gaseous product composition*

The gas composition differs with the pyrolyzed feedstock. The gas analysis results of experiments with the pure thermoplastics are listed in Table 3. An aliphatic dominance is visible in the gas composition from LDPE pyrolysis experiments. The light HCs are distributed over a chain length range from C_1 to C_{10}, with a maximum at C_3 and C_4 HCs. At 9.0 and 8.4 wt.%, 1-butene and n-butane are the main gases alongside propane, propene, ethane, and ethene. Linear n-alkanes and α-olefins also dominate in longer chain lengths. The gas composition in PP pyrolysis is similar to the LDPE results. However, a selectivity to propene (26.4 wt.%), iso-butenes (10.8 wt.%), and C_5 gases is detected. The C_5 gases are primarily composed of n-pentane (8.6 wt.%), 2-methyl-2-butene (3.9 wt.%), dimethyl-cyclo-propane (3.4 wt.%), and 2-pentenes (2.2 wt.%). Elevated quantities of 2-methyl-pentenes are also present (4.6 wt.%). In the polyolefin-based gases, the few aromatics, namely styrene and ethylbenzene, can probably be assumed to be artifacts from preliminary tests rather than having formed in the experiment. No heteroatom-containing HCs can be identified in the gas.

The composition of PS pyrolysis gas samples consists mainly of aromatics, as expected from other studies [15,30]. In addition to styrene (60.9 wt.%), toluene (9.8 wt.%), and benzene (4.7 wt.%), from Table 3, ethylbenzene (6.4 wt.%) and α-methylstyrene (1.4 wt.%) are quantified. Propylbenzene and cumene are also found in minor quantities. The low gas yield during PS pyrolysis complicates the gas analysis as the gas is

Table 3
Composition of pyrolysis gases generated in the experiments conducted with pure polymers in the STR at 500 °C wall temperature.

Gas species in wt.%[A]		LDPE	PP	PS	ABS	PA6	PVC
Light HCs	CH_4	4.3	4.0	0.0	2.7	4.2	0.7
(1st row: saturated; 2nd row: unsaturated)	C_2	9.7	7.8	0.3	2.7	4.0	0.5
		8.9	2.7	1.9	6.5	3.9	0.2
	C_3	10.7	6.0	0.1	1.2	2.6	0.3
		12.4	26.4	2.1	4.7	4.9	0.2
	C_4	8.8	1.8	0.1	0.6	1.8	0.2
		15.9	16.3	0.6	17.1	5.3	0.3
	C_5	3.9	12.4	5.2	0.3	2.2	0.2
		12.4	8.6	0.1	4.0	6.6	0.2
	C_6	1.3	0.6	0.0	0.5	0.3	0.1
		6.5	8.5	0.0	1.5	2.4	0.2
	C_7 to C_{10}	0.8	1.7	0.5	0.0	0.2	0.1
		1.4	2.5	4.8	0.5	0.6	0.1
Aromatics	Benzene	0.0	0.0	4.7	0.4	0.0	0.7
	Toluene	0.1	0.0	9.8	3.7	0.1	0.1
	Styrene	2.3	0.6	60.9	5.5	0.4	0.0
	Others aromatics	0.5	0.1	8.9	1.7	0.2	0.0
Heteroatom-containing gases	CO_2	0.0	0.0	0.0	3.3	47.3	10.7
	CO	0.1	0.0	0.0	0.2	9.3	0.2
	Other O-containing	0.0	0.0	0.0	0.0	0.9	0.2
	HCN	0.0	0.0	0.0	1.0	0.0	0.0
	Acrylonitrile	0.0	0.0	0.0	35.9	0.3	0.0
	Other N-containing	0.0	0.0	0.0	6.0	2.5	0.0
	HCl	0.0	0.0	0.0	0.0	0.0	84.1
	Other Cl-containing	0.0	0.0	0.0	0.0	0.0	0.7

[A] gas proportion related to the mass of entire permanent gas

diluted by a constant flow of flush gas. The concentration of some gas species reaches the limit for an adequate identification and quantification of the peaks. Also, the uncertainty and the influence of artifacts are higher compared to other gas samples of this study. The artifact impact is stronger because of the low amount of total gas. For example, the increased amounts of C_9 are presumably not formed as PS products but are rather attributed to artifacts of previous PP pyrolysis in the form of dimethyl-heptenes (4.0 wt.%) or the presence of 2-methylbutane (4.4 wt.%).

Similar gas species to PS experiments are obtained in the pyrolysis of the copolymer ABS. However, nitrogen-containing HCs and a relevant amount of HCN can be detected. The most prominent gases are acrylonitrile and acetonitrile with amounts of 35.9 and 6.0 wt.%, respectively. As a monomer in the ABS structure, acrylonitrile is expected, like the higher concentration of C_4 HCs. However, these C_4 HCs are mainly present in the form of butenes and not as butadiene, one monomer in the ABS structure.

Major amounts of CO_2 and CO form during PA6 pyrolysis. A few nitriles and multiple O-containing HC of low concentration are identified. The gas composition in PVC experiments is dominated by HCl and CO_2. HCl, as well as benzene and CH_4, which are also evident in the analysis, are known to be PVC's main decomposition components [31].

Table 4 lists the pyrolysis gas composition of the mixed plastics pyrolysis. Mix A only consists of aliphatic and aromatic hydrocarbons reflecting the feedstock composition, which comprises LDPE, PP, and PS. With Mix B, Mix C, and the PCW, gases generated from more complex feedstock compositions are analyzed. High amounts of CO_2 and CO are detectable. With more polyolefins in the mixtures, the gas composition shifts to higher concentrations of light aliphatic HCs. Only minor amounts of aromatics are detected. Heteroatom-containing gas species are identified. Reflecting the lower proportion of ABS, PA6, PET, and PVC in the feedstock, these values are significantly lower in Mix B than in Mix C or the PCW. Nevertheless, HCN is still present in Mix B with only 0.01 wt.%. For Mix C and PCW, the content of HCN amounts 0.06 and 0.03 wt.%, respectively. Chlorine- and oxygen-containing gases are also increased in Mix C and Mix B.

3.1.3. Composition of condensable products

The elemental composition of the pyrolysis condensates obtained in the STR is displayed in Table 5. The full data set and corresponding superposition calculations of the elemental analysis can be found in the supplementary information (S5). All condensates produced with the STR system contain a high carbon and hydrogen content ranging from 62.3 to 91.5 wt.% and 8.3 to 14.4 wt.%, respectively. The heteroatom content and the calorific value are highly polymer-dependent. The calorific value of LDPE, PP, PS, and plastic mixtures pyrolysis oils ranges from 42.1 to 46.6 MJ/kg. These values fit into the general range of reported

Table 5
Normalized elemental composition and calorific value of the pyrolysis oils obtained from pyrolysis of the investigated thermoplastics and thermoplastic mixtures in the STR system and superposition-based calculations.

Condensate	Elemental composition in wt.%					Calorific Value in MJ/kg
	C	H	N	Cl	O[A]	
LDPE	85.6	14.4	< 0.2	0.0	0.0	46.6
PP	86.1	13.9	< 0.2	0.0	0.0	46.3
PS	91.5	8.3	0.2	0.0	0.0	42.1
ABS	86.7	8.4	4.7	0.2	0.0	40.0
PA6	62.3	10.0	11.0	0.6	16.1	31.8
PVC	85.8	9.7	0.9	3.6	0.0	-[B]
Mix A	88.1	11.9	< 0.2	0.0	0.0	45.4
theo.[C]	87.9	12.0	0.1	0.0	0.0	-
Mix B	85.0	14.0	0.3	0.1	0.6	45.8
theo.[C]	84.7	13.8	0.2	0.0	1.3	-
Mix C	84.4	12.5	0.6	0.5	2.0	43.7
theo[C]	83.5	12.2	0.9	0.1	3.3	-
PCW	82.6	13.6	0.4	0.5	2.9	44.1
theo[C]	82.7	12.6	1.0	0.1	3.6	-

[A] calculated as the difference to 100 wt%.
[B] analysis not conducted because of high chlorine content.
[C] theoretical results estimated based on superposition calculations.

Table 4
Composition of pyrolysis gases obtained in STR experiments at 500 °C wall temperature and theoretical superposition-based calculations.

Gas species in wt.%		Mix A		Mix B		Mix C		PCW	
		exp.	theo.	exp.	theo.	exp.	theo.	exp.	theo.
Light HCs	CH_4	3.7		3.7		3.3		4.9	3.8
(1st row: saturated; 2nd row: unsaturated)			4.2		4.0		3.7		
	C_2	7.2	8.9	7.2	8.6	6.1	7.7	5.2	7.8
		5.6	6.2	6.6	7.0	7.1	6.3	7.0	5.9
	C_3	6.6	8.6	7.2	8.9	5.4	7.9	4.7	7.7
		19.1	18.4	12.8	14.5	9.8	12.9	10.3	14.8
	C_4	3.9	5.8	5.1	6.7	4.0	5.9	3.0	5.4
		13.6	16.0	11.7	14.8	9.4	13.5	9.5	13.9
	C_5	10.9	7.5	9.0	5.5	8.2	4.9	9.0	5.9
		11.0	10.7	7.9	10.7	7.7	9.6	7.2	9.6
	C_6	1.7	1.0	3.6	1.1	2.3	0.9	2.4	0.9
		11.2	7.4	7.5	6.5	7.3	5.8	9.6	6.2
	C_7 to C_{10}	0.6	1.2	1.1	0.9	1.1	0.8	0.9	1.0
		2.4	1.9	2.1	1.5	2.2	1.4	3.4	1.5
Aromatics	Benzene	0.5		0.2		0.7		0.6	0.1
			0.0		0.0		0.1		
	Toluene	0.5	0.1	0.3	0.1	0.7	0.1	0.5	0.1
	Styrene	1.0	1.7	3.3	1.8	0.4	1.7	0.4	1.5
	Others aromatics	0.4	0.3	0.4	0.4	0.3	0.4	0.3	0.3
Heteroatom-containing gases	CO_2	0.1		7.1		16.4		14.7	3.7
			0.0		2.4		3.7		
	CO	0.0	0.1	1.8	0.8	3.2	0.5	3.1	0.6
	Other O-containing	0.0	0.0	1.0	0.0	1.5	0.1	0.8	0.1
	HCN	0.0	0.0	0.0	0.0	0.1	0.0	0.0	0.0
	Acrylonitrile	0.0	0.0	0.0	0.0	1.1	0.4	0.5	0.3
	Other N-containing	0.0	0.0	0.0	0.0	0.5	0.2	0.6	0.2
	HCl	-	0.0	-	3.8	-	11.4	-	8.6
	Other Cl-containing	0.0	0.0	0.4	0.0	1.2	0.1	1.4	0.1

[A] gas proportion related to the total gas volume

data [12,13]. Chang et al. concluded a lower heating value of 45, 46, and 41–45 MJ/kg for PE, PP, and PS, respectively [12]. The calorific value of the mixed plastics corresponds well with the data summarized for the pyrolysis oil of mixed plastic waste [13]. They report a range of 40.5 to 45.6 MJ/kg [13].

In condensate of LDPE, PP, and PS experiments, no significant amounts of oxygen, nitrogen, or chlorine are detected. The polyolefins show a hydrogen/carbon ratio (H/C) of approximately 2.0. This finding is consistent with the expected aliphatic character of the LDPE and PP pyrolysis products. It corresponds to an H/C of about 1.8 and 2.0 for PP and PE reported by Calero et al. [25]. In contrast, an H/C of about 1.1 and 1.2 is calculated for the PS and ABS condensate, indicating mainly aromatic components. This value also corresponds to the H/C of 1.25 found in literature [25]. Nitrogen-containing compounds are also present in the ABS condensate. The highest content of HCs comprising nitrogen and oxygen is detected for the condensate generated from PA6. The condensate contains 16.1 wt.% of oxygen and 11.0 wt.% of nitrogen. This observation is consistent with the expected selective decomposition mechanism of PA6 to ε-caprolactam [32]. The low chlorine content in this sample may result from artifacts of previous PVC experiments. In PVC pyrolysis, a condensate with a high chlorine content of 3.6 wt.% chlorine is produced. Minor amounts of nitrogen artifacts from previous experiments also occur here. These artifacts complicate the interpretation of the results, but are hardly avoidable given the size and multistage setup of the pyrolysis condenser system in combination with the highly viscous condensates.

The condensate from Mix A contains only carbon and hydrogen as expected. The H/C is 1.6 and lies between the H/C of the condensate of individual polymers in the mixture. Mix B, Mix C, and PCW contain significant amounts of oxygen, nitrogen, and chlorine in addition to carbon and hydrogen. The nitrogen and chlorine content are significantly lower for Mix B (0.28–0.08 wt.%) than for Mix C (0.55 and 0.54 wt.%) and the PCW (0.43 and 0.53 wt.%). The oxygen content is also significantly lower for Mix B (0.6 wt.%) than for Mix C (2.0 wt.%) or the PCW (2.9 wt.%).

All condensates generated in the STR system are analyzed using the two-dimensional GC method. This allows for quantification of the main HC species and the compound groups. The results of the group evaluation are listed in Table 6. All chromatograms with indicated main compounds and the results of the main component quantification can be found in the supplementary information (S6).

Mostly linear aliphatic compounds are detected by two-dimensional GC in the LDPE condensate. These aliphatics are mostly comprised of unbranched n-alkanes and α-olefins. The condensable phase from PP pyrolysis, on the other hand, is composed of branched aliphatics. The most prominent component is 2,4-dimethylheptene at 3.7 wt.%. In both cases, the distribution extends over a broad chain length range, which is consistent with the results of the simulated distillation. Since the GC analysis method is technically limited for HCs with boiling points above 350 °C, a gap in the sum of quantifiable products prevents a complete analysis. This gap is not present for the PS condensate, as it mainly contains products in the analyzable boiling range. Mainly monoaromatics, diphenyls, and other aromatic compounds are quantifiable. A styrene concentration of 61.8 wt.% is determined. In addition, 2.5 wt.% ethylbenzene and 2.3 wt.% each of toluene and α-methylstyrene are found. α-Methyl-stilbene and triphenyl-cyclohexane form a pronounced blob in the chromatogram. Furthermore, a blob with very low intensity is recognizable, which is identified via MS as benzaldehyde. Because of uncertainties in the quantification methodology, the sum of all compound groups is 102.5. This result indicates a nearly complete characterization of the compounds in the pyrolysis oil within typical method deviations [28].

Condensates of the other pure plastics consist of many HCs that contain nitrogen, oxygen, and chlorine. In the ABS condensate, almost all of the 28.7 wt.% of heteroatom-containing HCs are nitrogen-containing substances such as benzobutanenitrile, 1-benzylpyrrole, or phenyl-pentenenitrile. Both aromatic and aliphatic nitriles are identified in relevant quantities. Fig. 5 shows the two-dimensional GC analysis of pyrolysis oil obtained by pyrolyzing ABS in the STR. HCs that have already been determined in the PS condensate are detected. The styrene concentration accounts for 31 wt.%. In addition, diphenylcyclopropane, α-methyl-stilbene, and triphenyl-cyclohexane are identified. ε-Caprolactam is also detected and is probably transferred to the condensate from previous PA6 experiments. It represents the main component in the PA6 condensate with approximately. 42 wt.%. of short-chain aliphatic nitriles, or short-chain and long-chain amides, are found in the PA6 condensate. Therefore, nitrogen- and oxygen-containing HCs can be detected exclusively. This requires fundamental adaptation of the compound group ranges, which are based on polyolefin-rich mixed plastic condensates.

However, for the PVC condensate, no group range adaptation is necessary. Increased concentrations of mono- as well as condensed and non-condensed polyaromatic compounds are detected. Only one prominent blob is recognizable, which can be specified as chlorine-containing HC. However, this blob, (1-chloroethyl)-benzene, emerges with high intensity. The analysis indicates small amounts of aliphatics. Palmitic acid and stearic acid, as well as smaller amounts of methyl palmitate and methyl stearate, are found. Small amounts of aliphatic HCs are detected. Benzobutannitrile and benzylpyrrole are found in the two-dimensional analysis of the PVC condensate, which can be attributed to the previous test with ABS, as already seen in the elemental analysis. However, due to the comparatively low condensate yield in the PVC test, their contribution to the composition is significantly higher than that of the PA6 artifacts in the ABS condensate.

The compound-group specific analysis for the mixtures is summarized in Table 7. The condensate of Mix A shows aromatic as well as branched and unbranched aliphatic components. Despite the blob of benzaldehydes, which also occurs in this mixture owing to the PS content, no heteroatom-containing HCs can be identified.

The two-dimensional GC chromatogram for the pyrolysis generated from the PCW is depicted in Fig. 6 as an example for the condensates of the mixed thermoplastic feedstocks. The condensates of Mix B, Mix C, and the PCW contain mostly aliphatics with 69.7, 52.6, and 56.2 wt.%, respectively. Nevertheless, monoaromatics and especially diphenyls and polyaromatic structures are also evident. The composition of the PCW condensate is similar to that of Mix C. At 3.5 wt.%, the heteroatom-containing HCs in the PCW condensate are slightly higher than in the condensate of Mix C. The previously determined main components of ABS, PA6, and PVC pyrolysis are detectable at lower intensities. In addition, benzoic acid is detected in the condensates from Mix B, Mix C, and PCW. The proportion of benzoic acid in the condensates amounts to 0.50 and 0.84 wt.% for the condensate from Mix B and Mix C. In the PCW, additional blobs are detectable as C_{13} and C_{14} nitriles, as well as aliphatic oxygenated compounds.

Table 6
Compound group-specific GC analyses of the pyrolysis oils obtained from pyrolysis of pure thermoplastics in the STR system.

Compound group	Content of compound group in the pyrolysis oil sample in wt.%					
	LDPE	PP	PS	ABS	PA6	PVC
Aliphatics	73.9	78.3	4.4	2.1	0.3	6.4
Monoaromatics	2.0	2.3	69.8	42.4	0.2	6.7
Indenes	0.1	0.0	0.1	0.2	0.1	1.2
Naphthalenes	0.1	0.0	0.1	0.7	0.1	1.2
Diphenyls	0.4	0.3	13.6	6.1	0.6	6.1
Other aromatic compounds	0.4	0.3	13.7	6.1	0.0	11.8
Heteroatom-containing HCs	0.0	0.1	0.8	28.7	67.7	11.0
Sum of identified compounds	76.9	81.3	102.5	86.3	69.0	44.4

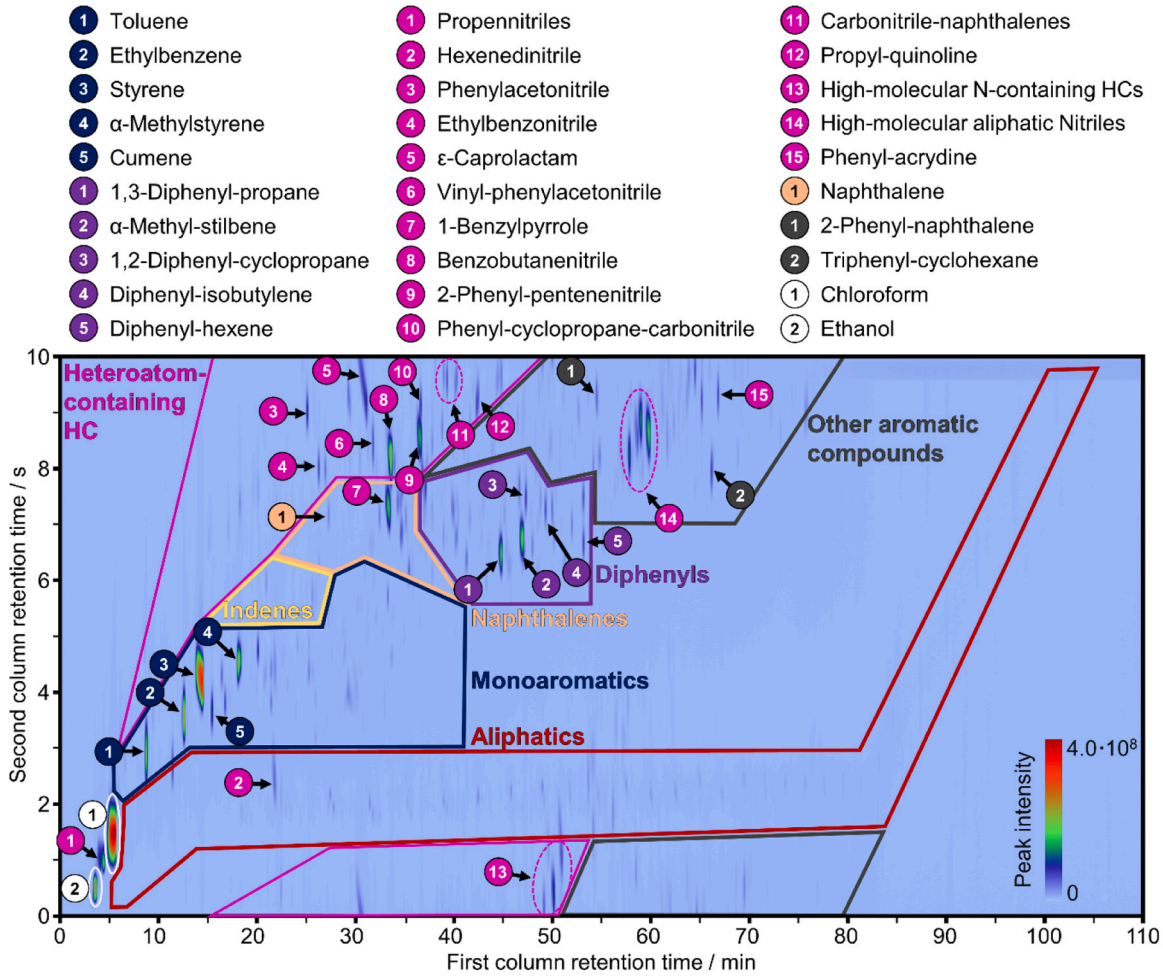

Fig. 5. Chromatogram of the condensate obtained during ABS pyrolysis in the STR system.

Table 7
Compound group-specific GC analyses of the pyrolysis oils obtained by pyrolysis in the STR system and the superposition-based calculated analysis for Mix A condensate.

Compound group	Content of compound group in the pyrolysis oil sample in wt.%				
	Mix A	Mix A (theo.)[1]	Mix B	Mix C	PCW
Aliphatics	50.2	49.3	69.7	52.6	56.2
Monoaromatics	25.5	27.2	3.3	13.5	6.1
Indenes	0.2	0.1	0.1	0.2	0.1
Naphthalenes	0.2	0.1	0.1	0.2	0.2
Diphenyls	3.8	5.2	1.0	1.8	1.1
Other aromatic compounds	3.6	5.3	1.2	1.4	0.9
Heteroatom-containing HCs	0.4	0.3	1.2	3.0	3.5
Sum of identified compounds	83.9	87.5	76.6	72.7	68.1

[1] superposition-based calculation considering polymer content in the feedstock and condensate yields.

3.2. Comparison of the STR and ASR pyrolysis system

The conducted investigations allow the comparison of the STR pyrolysis results with those of pyrolysis in the ASR system. The previously presented mass balances and product compositions of gas and condensate fractions of the STR system serve as comparison parameters to the ASR results.

3.2.1. Product yield comparison

In Fig. 7, the mass balances of pure thermoplastics and thermoplastic mixtures are compared to the available data from the ASR study [23]. As for the STR experiments, each feedstock was pyrolyzed at least twice in the ASR system. The condensate yields are significantly higher in the STR for LDPE, PP, and PS. Solid residues are negligible. In experiments with these pure polymers, the ASR yields less condensate of only 48.8, 49.1, and 88.5 wt.%, respectively. Consequently, it shows higher permanent gas yields.

Reactor-specific differences also emerge when comparing the mass balances for the thermoplastic mixtures. Compared to the STR, a lower condensate yield can be observed for pyrolyzing Mix A in the ASR system, as is the case when comparing the pure materials. Despite measurement inaccuracies of 1–3 wt.% of the condensate yields, this tendency is also identified for the yields of the mixtures Mix B, Mix C, and PCW. The condensate yield in the STR is 5.8, 5.6, and 2.6 wt.% higher, respectively. However, the trend is significantly less pronounced for the heteroatom-containing thermoplastic mixtures than for pure thermoplastics.

3.2.2. Comparison of gaseous products

The impact of reactor design is also evident when comparing the gas composition obtained in both reactor setups. The detailed results of the ASR experiments are provided in the supplementary information (S4). The gas from LDPE, PP, PS, and Mix A experiments shows similarity to the results of the ASR experiments. The HC distribution reveals a slight shift towards short-chain HCs at the STR for polyolefinic feedstocks. For the other feedstocks, lower aromatic contents can be quantified in the

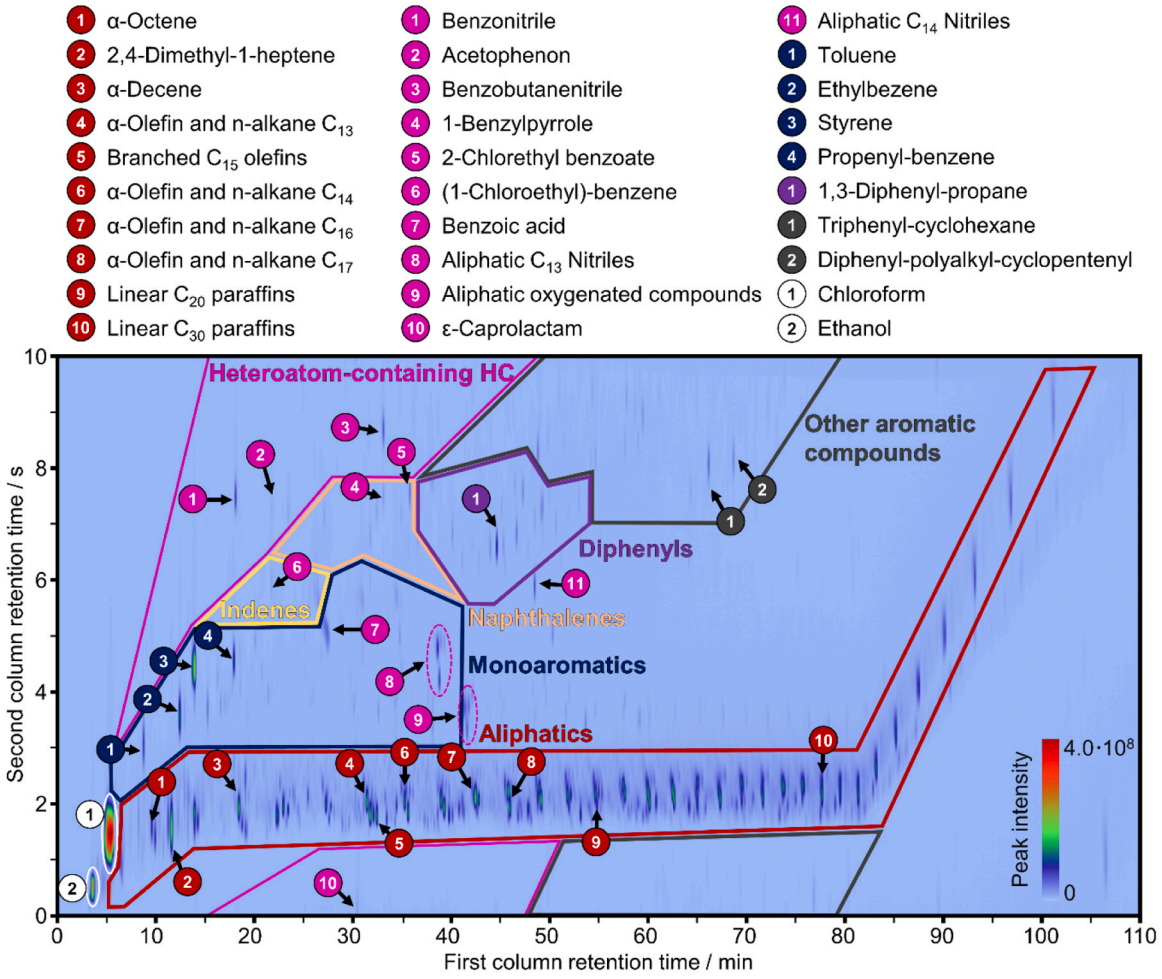

Fig. 6. Chromatogram of the condensate generated from PCW pyrolyzed in the STR system.

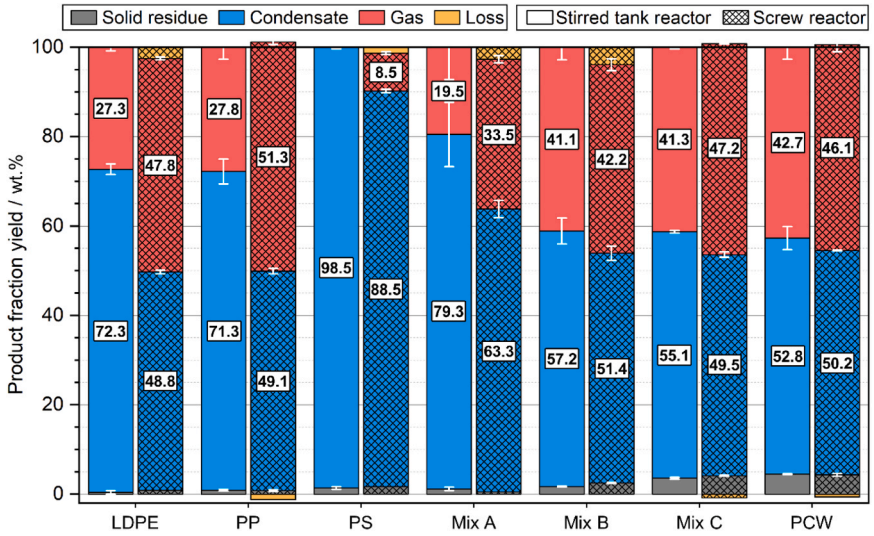

Fig. 7. Mass yields of the pyrolysis experiments with thermoplastics at 500 °C reactor wall temperature in the STR system (plain) compared to ASR results (shaded) [23].

product gas obtained from STR experiments.

Comparing the gas analyses of the heteroatom-containing feedstock experiments, less heteroatom-containing HCs are detected in the ASR than in the STR. For example, a lower concentration of CO_2 (4.4 and 7.7 wt.%) and CO (1.0 and 1.5 wt.%) is obtained in the ASR system for the pyrolysis of Mix B and the PCW, respectively. Comparisons regarding Mix C cannot be provided as comprehensive data for the pyrolysis of tis feedstock in the ASR is missing.

3.2.3. Comparison of condensable products

The condensate analysis also reveals strong variations related to the reactor type. Fig. 8 depicts the condensates' elemental analyses obtained at the ASR in comparison to the results of the STR. The ASR condensate characterization is presented by Netsch et al. in a previous work [28]. The results are summarized in the supplementary information (S5) in detail. No significant differences are evident for the condensates obtained from LDPE, PP, PS, and Mix A, in contradiction to the heteroatom-containing polymer blends.

The carbon content in the condensates generated from Mix B, Mix C, and the PCW at the STR is significantly lower, while the hydrogen content is higher, resulting in a higher H/C in the condensates produced from Mix B, Mix C, and PCW of 2.0, 1.8, and 2.0, respectively. The H/C of the corresponding condensates obtained in the ASR are 1.8, 1.6, and 1.7. The comparison of the mixed plastic condensate for both reactors also reveals distinct contrasts relating to the oxygen content. In the condensates of the reference mixtures and the PCW that were produced in the STR, significantly higher oxygen and lower carbon content are determined. The increase in oxygen is less pronounced for Mix B. Mix C and the PCW condensate exhibit higher oxygen contents of 2.0 and 2.9 wt.% than the corresponding condensate from the ASR, accounting for 0.9 wt.% of oxygen, respectively. For nitrogen and chlorine, no significant trends are apparent for the three mixtures pyrolyzed in both reactor types.

The condensates obtained from the STR reactor were analyzed by two-dimensional gas chromatography and compared to the corresponding reported data by a previous study at the ASR system [28]. The detailed elemental compositions are provided in the supplementary information (S5). The same blobs can be seen in chromatograms of polyolefins and polystyrene condensate. However, the compound proportions shift slightly towards shorter retention times and thus molecules with low molecular weight. This observation is much more pronounced in condensate obtained from PS than from polyolefins. The two-dimensional GC analyses, cannot verify the increase in oxygen-containing species for the STR condensate from Mix B, Mix C, and the PCW.

While elemental and GC analyses provide a general overview of heteroatom impurities, they cannot reveal the entire condensate composition in terms of molecular weight distribution. In particular, the analysis of the boiling point distribution can serve as an indicator for this characteristic condensate property. Furthermore, it provides important key parameters for further utilization of the condensates in chemical processes. The condensate of the polyolefins, PS, and the mixtures pyrolyzed in the STR were analyzed. The results are shown in the diagrams in Fig. 9. All condensates differ but cover a broad boiling range, including common petrochemical boiling cuts such as naphtha, middle distillate, and vacuum gas oil (VGO). The initial boiling point is at about 50 °C, and the final boiling point reaches 650 °C in maximum. The PE and the polymer mixtures' boiling curves exhibit the lowest proportion of naphtha cut. The PP curve shows a significantly lower boiling point in the range of 5 to 90 wt.% of distilled mass. In the styrene boiling curve, distinct horizontal lines at 145–150, 295, and 382 °C are visible. For Mix A, the styrene-indicating plateau remains visible. The distilled sample mass covered by the plateau accounts for about 20 wt.%. The rest of the curve is similar to that of LDPE and PP and extends over a broad boiling range. Condensate of Mix B and Mix C obtained from the STR system exhibits similar characteristics to LDPE condensate. This is expected from the LDPE content of 70 and 50 wt.%, respectively. Compared to condensate generated from Mix B, Mix C shifts slightly towards smaller molecular weights as a result of the lower LDPE content. The simulated distillation curve of the PCW condensate from the STR system differs minimally from these reference mixtures.

The simulated distillation curves of the condensate generated in the ASR system is also depicted in Fig. 9. For LDPE and PP, the curve is drastically shifted towards a lower boiling point compared to the STR results. Approximately 32 and 36 wt.% more naptha-range product cuts are visible in the ASR condensate, respectively. The condensable product fraction from PS experiments in the ASR shows a similar proportion of the styrene-indicating horizontal plateau. Nevertheless, more compounds with boiling points below 140 °C are detected. Comparing Mix A, Mix B, Mix C, and the PCW condensate, the shift towards low-boiling products becomes even more significant.

4. Discussion

4.1. Feedstock influence

The results emphasize the feedstock influence in plastic pyrolysis. This influence on the pyrolysis behavior is discussed by highlighting the differences between pure polymers and examining mixed thermoplastics.

4.1.1. Pure polymer behavior

The preliminary validation of mass balancing with MgOX proves the reliability of the applied methodology and the generated data. The comparison of different plastic types pyrolyzed in the STR demonstrates the strong contrasts in their pyrolysis behavior.

The polyolefins pyrolyze following a statistically distributed radical

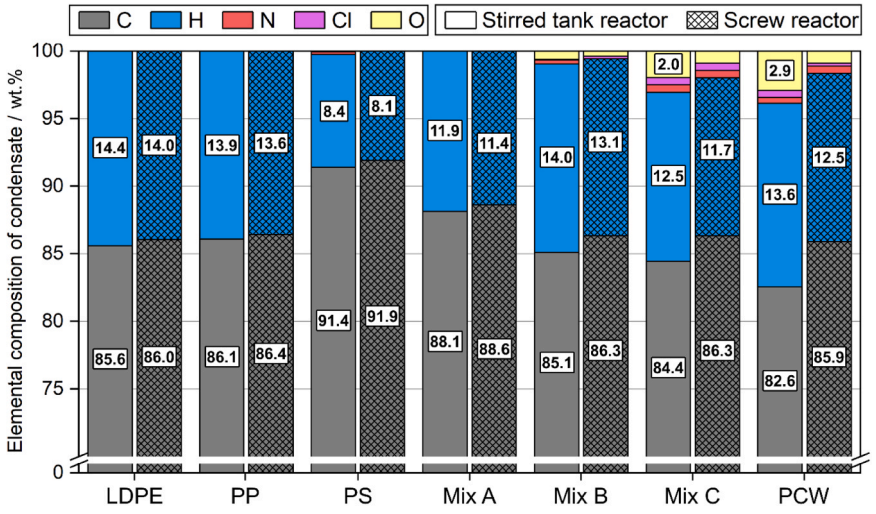

Fig. 8. Elemental composition of the pyrolysis condensate obtained at 500 °C reactor wall temperature in a STR (plain) and the ASR system (shaded; adapted from Netsch et al. [28]).

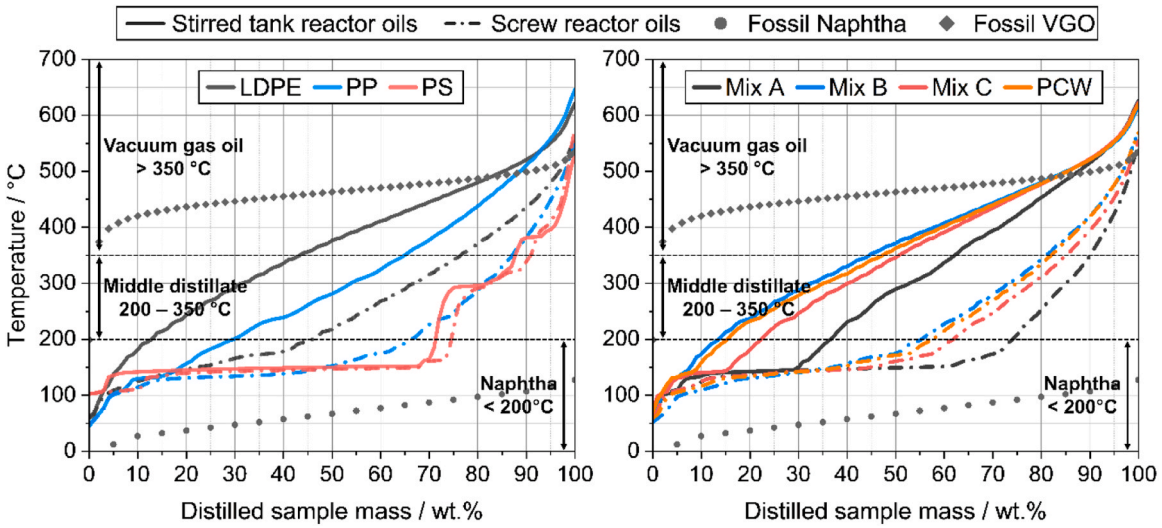

Fig. 9. Simulated distillation curves of the analyzed STR pyrolysis condensates compared to ASR results (adapted from Netsch et al. [28]) alongside fossil benchmark examples of naphtha (adapted from [33]) and VGO (adapted from [34]).

chain mechanism, leading to a broad product distribution of long-chain aliphatics [35]. The gas composition quantified for LDPE and PP pyrolysis meets the expectations drawn from reports by other authors [15,17,35]. An increased content of high-boiling gas species can be detected. However, other studies have not quantified components higher than C_4 in the pyrolysis gas [19,20]. This difference could be caused by more efficient condensation systems in their reported experimental setups or in the lower resolution of their analyses. The number of potential HC configurations increases significantly with increasing chain length. Consequently, the respective concentrations become comparatively small. In these studies, pyrolysis gas is analyzed using a micro GC instead of a high-resolution GC system. Therefore, the combination of FID and MS in this study's GC method allows the identification and quantification of such less pronounced peaks over a broad range of chain lengths. The advantage of this system is also evident in the gas analyses of other experiments with different polymers. The results of the condensate analysis align with the product yields and the gaseous product. No heteroatoms are present, and the highest H/C is achieved in the LDPE and PP pyrolysis oil, making polyolefins the ideal feedstock for chemical recycling plants. Only unbranched α-olefins and n-alkanes dominate the composition of LDPE condensate, which extends over a broad boiling range. The simulated distillation curves depicted in Fig. 9 emphasize the broad molecular weight distribution of aliphatics in the PE condensate. This is consistent with the reported formation of waxes at lower pyrolysis temperatures [8,35]. Following the decomposition mechanism of PP, the analyzed distribution is concentrated in the range of lower boiling temperatures.

The selective decomposition mechanism of PS feedstocks to styrene and its oligomers explains the high condensate yield [30]. The gaseous and condensable products confirm the presence of high amounts of PS monomer, its dimers, and its trimers. No specific dimer or trimer structure of PS can be found in the condensate. Rather, there are many different dimer- and trimer-like derivatives present. Nevertheless, condensed aromatic structures are found, giving examples of byproducts in the selective PS decomposition mechanism. The occurance of benzaldehyde is not expected, given the chemical structure of PS. It is therefore attributed to impurities from the manufacturing process or to small amounts of additives in the polymer. The horizontal lines in the PS curve align with the presence of specific molecules of styrene, its dimers, and its trimers. The temperature of these horizontal lines of about 145–150, 295, and 382 °C corresponds to the monomer, dimer, and trimer evaporation temperatures.

ABS results are similar to PS pyrolysis yields and composition. The additional butadiene and nitrile components in the co-polymer configuration of the ABS lead to the formation of pyrolysis gas [36], rich in butenes and acetonitrile and acrylonitrile. The presence of diphenyl-cyclopropane, α-methyl-stilbene, and triphenyl-cyclohexane also corresponds to the copolymer structure of ABS with aliphatic parts from butadiene and aromatic polymer parts. The chemical composition of the ABS condensate matches literature values for pyrolysis products of ABS [36]. The significant amounts of nitrogen in the condensate in the form of nitriles, quinolines, or pyrroles are expected to pose a problem in chemical recycling applications.

PA6 pyrolysis is reported to feature a selective decomposition mechanism to the monomer ε-caprolactam [32]. Because of its thermophysical properties, this monomer accumulates in the condensate. This explains the high condensate yield in PA6 pyrolysis determined in this study. With an ε-caprolactam content of approximately 42. wt.%, considerably less monomer is generated than compared to relevant studies in the literature [32]. The pronounced CO_2 formation during PA6 pyrolysis indicates a partial cleavage of the amide bonds of the PA6 backbone, resulting in the formation of other gas species. Consequently, HCs in the range of C_1 to C_6 are detectable in nearly evenly distributed amounts. This strengthens the assumption that under the experimental conditions, secondary cracking of ε-caprolactam occurs, reducing the overall monomer content. The absence of higher HCs strengthens the assumption of minor relevance of repolymerization reactions in the STR setup. These species are only expected if repolymerization or comparable addition reactions occur between unsaturated HCs of the gas phase.

The product yields of the PVC pyrolysis are consistent with a summary of PVC decomposition behavior by Yu et al. [31]. The reported two-stage PVC decomposition mechanism features preferential HCl formation in a first step and coke formation in a consecutive reaction of high-molecular polyene chains. Comparing the coke yield of 17.0 wt.% determined by incineration to the total amount of solid residue (28.9 wt.%), a difference is detectable. This difference is probably caused by the fillers contained in the PVC. The feedstock analysis reveals an ash content of about 12 wt.%. About 10.3 wt.% of this content are assigned to $CaCO_3$ and TiO_2 fillers by the manufacturer. TiO_2 is chemically stable in the relevant temperature range [37]. The composition of PVC pyrolysis gas includes high amounts of CO_2 and CO. CO_2 may only be formed via air exposure during pyrolysis or additives contained in the feedstock. Air entry can be excluded in this study, as the experimental methodology ensures a completely inert atmosphere in the reactor. Thus, their detection might also refer to the presence of fillers in PVC. The

decomposition of pure $CaCO_3$ to CO_2 and CaO starts at temperatures above 600 °C in an inert atmosphere [38]. However, Paydar et al. describe the decomposition of $CaCO_3$ happening at lower temperatures in the presence of HCl [39]. Therefore, interaction effects between filler and polymer emerge as a potential cause for the formation of CO_2. Furthermore, oxygen-containing additives may also degrade during pyrolysis and release light oxygenated hydrocarbons. Other chlorine-containing HCs, such as chloromethane, chloroethane, chloroethene, chlorobutane, and dichlorocyclopropane, are identified in small quantities. The chlorine content in PVC condensate accounts for 3.6 wt.%. An experimental study with PVC in a furnace reactor revealed a significantly lower chlorine content in the oil of 0.16 wt.% [25]. Also, the authors report an oxygen content of 31.3 wt.% [25]. This finding, together with the elemental analysis of their feedstock, strengthens the presumption of additives that are incorporated in the PVC used in their study. The PVC employed in this study features a significantly lower amount of oxygen, which might explain the differences from the reported data. The oxygen content can be attributed to the palmitic and stearic acids identified via two-dimensional GC. Most probably, palmitic and stearic acids are not formed during pyrolysis, but rather represent additives contained in the PVC that volatilize during the pyrolysis process. Unexpectedly, only one specific chlorine-containing HC can be detected in the PVC condensate by two-dimensional gas chromatography. Chlorine atoms may be distributed across numerous different molecules with low intensities or high boiling points, making them difficult to identify in GC. However, aliphatic compounds are present. The presence of aliphatics may indicate that the polyene chains, which are formed as intermediate products [31], may not completely form aromatic structures, but also pass into the liquid product as unsaturated aliphatics.

4.1.2. Pyrolysis of mixed plastics

The strong feedstock influence is evident in the pyrolysis of the polymer mixtures. The yields of product fractions reflect the proportions of the yields of the incorporated individual polymers. Interaction effects can be assessed by applying the superposition approach to calculate theoretical product yields and product composition.

The calculated product yields for Mix A amount for 79.9 wt.% of condensate and 19.3 wt.% of the pyrolysis gas. They are consistent with the experimental results. Consequently, interactions between LDPE, PP, and PS that significantly change the overall product yields are not evident. This aligns with expectations based on laboratory-scale kinetic studies [11]. Applying the superposition calculation approach to the gas analysis, a similar composition can be calculated compared to the experimental results. Only minor differences of 3 wt.% in maximum are determined. Theoretical calculation of the elemental analysis results for Mix A reveals consistent findings. The carbon and the hydrogen content amount to 87.9 and 12.0 wt.%. The two-dimensional GC analyses show aromatic as well as branched and unbranched aliphatic components reflecting the LDPE, PP, and PS content in the feedstock. The content of aliphatics and monoaromatics differs only slightly at 0.9 and 1.7 wt.%. Diphenyls and other aromatic components are slightly overestimated. Considering measurement inaccuracies, the calculated compound groups also correspond well to the experimentally determined values. The condensate composition from Mix A appears suitable for chemical recycling applications, given its low heteroatom content. However, they still contain a high level of aromatics as a result of the high PS content in the feedstock, which must be considered during downstream pyrolysis oil processing. Generally, the STR results emphasize the possibility of calculating the product yields, as well as gas and condensate compositions for mixtures of LDPE, PP, and PS.

This conclusion does not apply to mixtures containing heteroatoms. The pyrolysis of these feedstocks results in similar product distributions independent of the polymer proportions. The slight increase in solid residue of PCW pyrolysis compared to Mix C might also be attributed to the presence of inorganic components, such as fillers. This corresponds with the determined ash contents of the feedstocks in Table 1. The species in the gaseous product fraction of the pyrolyzed plastic mixtures can be referred to the specific polymer types. The intensive CO_2 and CO formation is known from the PA6 and PVC pyrolysis. Also, PET decomposition is known for its formation of CO_2 and CO in high quantities [15]. Because of the low gas yield of PS and ABS, minor proportions of aromatics are detected in the gas phase.

The condensate produced from Mix B, Mix C, and the PCW mainly consists of aliphatics and exhibits a comparatively low aromatic content. This relates to the low proportion of PS, ABS, PVC, and PET compared to Mix A. Heteroatom-containing HCs are detected in the condensate product of Mix B, Mix C, and the PCW via two-dimensional GC. The detected nitrogen- and oxygen-containing HCs in the mixtures extend over a broad chain length range and are bound in aliphatic as well as aromatic structures. Additional blobs in the PCW condensate, detectable as C_{13} and C_{14} nitriles, cannot be assigned to specific polymers tested individually. Consequently, they are assumed to originate from additives or other waste components contained in the polymers of the PCW. For example, certain additives may evaporate directly, similar to palmitic acid and stearic acid in PVC, or pyrolyze, leading to the formation of such compounds. The minor differences between the distillation curves of Mix C and the PCW condensate show that additives that may be present in the feedstock appear to have minimal influence on the condensates' boiling behavior. This is in line with the GC analyses. The potential additive-related compounds were only identified as trace substances. The total amount of oxygen in Mix C and PCW condensate is quantified to 2.0 and 2.9 wt.% by elemental analysis. Alongside the nitrogen and chlorine content in the samples, a higher proportion than 3.0 and 3.5 wt.% of heteroatom-containing HCs is expected from the two-dimensional GC. The selective enrichment of oxygen in compounds of the HC with elevated evaporation temperature may be possible and explain this finding. Compounds that contain chlorine and nitrogen may accumulate in this high-boiling distillation cut. Further research on the chemical composition of the high-boiling compounds in the condensate is required for final clarification. Kusenberg et al. provide a comprehensive overview of the nitrogen, chlorine, and oxygen content analyzed by various authors for different plastic mixtures [40]. Their review indicates the tendency that high amounts of a contaminant in the feedstock increase the corresponding content in the pyrolysis oil. They report a maximum content of 0.36 wt.% nitrogen, 3.8 wt.% oxygen, and 1.4 wt.% chlorine in the pyrolysis oils [40]. The results of this study correspond with the author's findings. From the elemental composition, high amounts of polyolefins in the pyrolyzed feedstock are advantageous, referring to the heteroatom content. On the other hand, the simulated distillation reveals a possible disadvantage of high LDPE content, as it shifts the condensate composition towards high-molecular-weight compounds under the experimental conditions conducted in the STR experiments. Generally, the determined levels of heteroatom content impair further reintroduction of the mixed plastic oils into petrochemical processes. Thus, subsequent upgrading of the condensates would be required.

4.1.3. Polymer interactions in mixed plastics

Superposition calculations reveal decisive interaction effects when coprocessing the heteroatom-containing polymer mixtures. To estimate yields for Mix B, Mix C, and the PCW by superposition PET data is missing. Therefore PET product yields determined by Genuino et al. [29] are used. Following the PET study, a yield of condensate, gas, and solid residue for PET of 55, 13, and 32 wt.% is assumed. Applying these assumptions for calculations, Mix B and Mix C result in a condensate yield of 70.8 and 71.1 wt.%, respectively. These yields are about 20 and 22 wt.% higher than the experimentally determined results, emphasizing the dominant product shift from condensable to gaseous products because of interactions. The theoretical condensate yield of the PCW (69.9 wt.%) is also overestimated by about 19 wt.%. Similar findings concerning the overestimation of condensate yields based on the

superposition approach are reported by Genuino et al. [29]. The authors attribute these results to the interaction effects of PET with other polymers, indicating an overestimation by up to 8 wt.% in their study. Further studies show that the interactions are also involved in the co-pyrolysis of the heteroatomic polymers PVC and PA6 [11]. The interactions are specified in more detail, for example, by Cao et al. for a defined feedstock system of PVC and PET [41]. In the proposed reaction mechanism, reactions occur between evolving HCl and the intermediates of PET decomposition, more specifically, the aromatic ester fragments. Gaseous chlorinated HCs, like ethylene dichloride or ethylene chloride, form instead of HCl. This mechanism explains the increased gas yields and the reduction of the condensate amount. Similar interaction effects for PVC and PA6 appear reasonable, but require further investigation. The comparison of experimental and calculated results for thermoplastic mixtures in this study cannot confirm an increased tendency towards coke formation, as found by Genuino et al. in a fixed-bed reactor. They attributed an increase in solid residue formation of up to 18 wt.% to the interaction effects of PET with other polymers. The discrepancy between the two studies highlights the need for fundamental research into the interaction effects regarding the dependence on feedstock composition and reactor characteristics.

For the superposition-based estimation of the gas composition from the heteroatom-containing feedstocks, literature data of the PET pyrolysis gas composition are required. Honus et al. provide comprehensive data on the PET pyrolysis gas composition [15]. The authors report a composition comprising 64 wt.% CO_2, 31 wt.% CO, 2.8 wt.% ethylene, 0.6 wt.% CH_4, 0.5 wt.% benzene, 0.5 wt.% toluene, 0.25 wt.% propene, 0.2 wt.% ethane, and 0.15 wt.% butene. With this data, the occurrence of interactions can be verified for Mix B, Mix C, and the PCW. The experimentally determined amounts in the gas composition of Mix B, Mix C, and PCW differ from the superposition-based calculations. Fewer aromatics and slightly fewer light olefins are included in the normalized composition. Approximately 1–3 wt.% more C_6 aliphatics are formed than could be predicted by superposition calculations. The experimentally determined amounts of heteroatom-containing HC, CO, and CO_2 in the gas composition exceed the calculated results by far. In particular for Mix C, which has the highest heteroatom content of all feedstocks, an additional 3.6, 12.3, and 11.0 wt.% of these gas species are determined. Therefore, oxygen-, nitrogen, or chlorine-containing polymers appear to pursue new reaction pathways leading to more heteroatom-containing HCs, CO, CO_2, and C_6 aliphatics in the gas while diluting aromatic and aliphatic gas species. For example, the reaction mechanism of PA6 could change in a way that the usual highly selective ε-caprolactam formation changes into decomposition to short-chain aliphatics, nitriles, CO, and CO_2. Further mechanistic insights into such changes cannot be resolved with this experimental setup.

Consistent with the previous calculations, the superposition principle is only partially applicable to the elemental composition of the mixed plastic condensates. The carbon and hydrogen content represented within the measurement uncertainty, considering simplifications by using pure PET tests from the literature [25]. However, the chlorine content is underestimated (by 0.4 wt.%), while the oxygen and nitrogen content are slightly overestimated by up to 0.6 and 1.3 wt.% for Mix C and the PCW. As discussed in the previous section, interactions appear the have a major influence on the product composition. As described before, interactions leading to the release of low molecular weight chlorinated HCs are reported [41]. The underestimated chlorine content indicates that HCl from primary PVC decomposition may be integrated into higher boiling HC structures during reactions with the PET and PA6 intermediates. Chlorinated polyaromatic hydrocarbons could play a dominant role in this process. As a result of the increasing cleavage of heteroatom-containing polymer chains caused by the interaction with HCl, more gaseous nitrogen- and oxygen-containing HCs, such as acrylonitrile, acetonitrile, or acetaldehyde, seem to be formed. The more pronounced formation of CO_2 and CO would explain the reduced oxygen content in the condensates. Also, it would explain the underestimation of chlorine-containing HC by 1.3 m.% in the gas superposition calculations and the overestimation of chlorine by 0.4 m.% in the condensate phase. With this data, significant interactions during the pyrolysis of Mix B, Mix C, and PCW assumed from the gas analysis, are confirmed. Unfortunately, the gas measurement method does not allow the HCl content in the mixed plastics to be recorded. A decreasing amount of HCl in the gas phase would offer an additional validation possibility for the assumed interaction effects. The superposition calculations for the compound group distribution of the heteroatom-containing feedstocks are impossible, as adequate data for the PET condensate is not accessible in the literature. However, based on previous observations, it cannot be assumed that the superposition approach is valid for calculating the composition of Mix B, Mix C, and PCW.

4.2. Reactor impact

The comparison of the pyrolysis results generated in the STR and the ASR system allows for evaluating the reactor impact. The reactor impact is underlined by significant differences in the obtained product yields. Compared to the STR, the mass balance shifts significantly in favor of the gaseous products. This shift is attributed to differing reactor characteristics caused by the reactor geometry and technical operation. The GRT is considerably lower in the STR system. The potential for secondary reactions is therefore reduced compared to the ASR system. Secondary cracking of volatiles in the gas phase is less likely to occur in the STR. Additionally, the shift from condensable to gaseous products may be attributed to the time-dependent variations of the polymer temperatures. In the STR, the polymer end temperature is assumed to be lower than in the ASR, which would reduce the intensity of cracking reactions. Nevertheless, the lower heating rate in the ASR probably causes the polymer to react already at lower temperatures. Accordingly, a product distribution shift caused by the time-dependent temperature profile of the reacting polymers cannot finally be clarified. However, the GRT comparison of both reactor systems provides a comprehensible explanation for the effect of shifting yields.

When comparing this effect for different feedstocks, the effect is significantly weaker for mixtures containing heteroatoms. As described in the previous section, strong interaction effects between the polymers are noticeable in these mixtures. These interaction effects appear to superimpose and dominate the specific plant characteristics, such as temperature distribution and GRT. Regardless of the reactor type and plant design, more even product yields are achieved for the heteroatom-containing mixtures. The feedstock-specific interactions appear to be decisive for the pyrolysis yields in the compared reactor systems.

In combination with the observed lower gas yields, the gas analyses indicate less pronounced thermal cracking reactions in the STR reactor. Secondary thermal cracking is presumably intensified in the ASR system with longer GRT in the hot reactor section. The total amount of products with boiling points ranging from C_4 to C_7 is therefore increased, which may cause a higher content of these products in both fractions. However, for the pyrolysis gas of Mix B and PCW, the heteroatom-containing HCs are more pronounced in the STR system. This might also be attributed to less intense primary and secondary cracking in this reactor. As seen before, fewer gaseous HCs are formed compared to the ASR. The formation of heteroatom-containing gas species like CO, CO_2, or light nitriles is presumably less influenced by temperature variations than HCs that evolve during the polyolefin decomposition mechanisms. As a result, the other heteroatom-containing gases are diluted to a lesser extent.

The condensate analyses indicate further effects depending on the reactor type. For LDPE, PP, PS, and Mix A, the elemental composition of the pyrolysis oils remains unaffected. This result is expected, as evolving products may change regarding the chain lengths or the distribution between styrene monomer, dimer, and trimer, but do not modify the fundamental structural nature of the evolving products.

For Mix B, Mix C, and the PCW, the H/C ratio differs slightly by up to

0.3. Given the mostly polyolefin-rich feedstock composition, this indicates fewer unsaturated bonds in the condensates of the mixed plastics in the STR. This may be caused by a lower tendency to form unsaturated organic compounds, resulting from less pronounced aromatic formation as a secondary reaction. More likely, primary and secondary cracking are intensified in the ASR system, reflecting the longer GRT and the presumably higher average polymer temperature. Regarding the heteroatom content in the condensate, no significant changes are evident when comparing the condensate of both reactors, except for oxygen. The condensates produced in the STR have a slightly higher oxygen content. This slight increase could be related to measurement uncertainties and is inconsistent with the identified effect of increased CO_2 and CO levels in the STR system. The two-dimensional GC analysis shows no significant variation in oxygen-containing structures, supporting the assumption that the oxygen difference observed in elemental analysis is attributable to measurement uncertainties. On the other hand, the technical limitations of the GC method may cause this result. High-boiling oxygen-containing compounds in the condensate may be discriminated in the two-dimensional GC method. Since the method does not cover any or only partial components with an elevated boiling temperature of over 350 °C, high-boiling compounds with oxygen-containing structures are presumably undetected. Terephthalic acid, a typical product of PET pyrolysis with a sublimation temperature of 405 °C, would be an example of this. A final clarification of the oxygenated HCs requires further investigations, such as a distillative separation combined with an analysis of the distillation fractions for possible heteroatom enrichments. The results will further support the evaluation of interaction effects in the mixed plastic pyrolysis. Nevertheless, upgrading the pyrolysis condensates from the mixed plastics is necessary independently of the reactor type, considering common specifications for petrochemical products [40].

The two-dimensional condensate analysis confirms the shift towards a condensate distribution with fewer high-boiling compounds in the ASR system. The distribution of products in LDPE and PP condensates is shifting toward shorter chain lengths. Nevertheless, it is still very broad. The styrene content in the PS condensate is about 10 wt.% higher in the STR system compared to the sample generated in the ASR system. In literature, higher styrene yields are linked with increased reactor temperatures [30], which contradicts the assumption of a presumably higher polymer end temperature in the ASR system. However, the longer GRT in the ASR may lead to more pronounced gas phase reactions, interfering with the selective PS decomposition mechanism. This would explain why the amount of other monoaromatic structures, such as ethylbenzene, toluene, or α-methylstyrene, is significantly higher in samples of the ASR system, while the styrene content is lower. The sum of monoaromatic structures remains nearly constant in both samples. These findings confirm the hypotheses that the ASR geometry and operation procedure lead to more intense secondary gas-phase cracking reactions.

The comparison of the simulated distillation confirms this hypothesis of enhanced cracking in the ASR. The intensified primary and secondary cracking reactions result in more unsaturated aliphatic compounds of shorter chain length, considering the mostly polyolefinic character of the mixtures. The unsaturated bond of the typically formed α-olefins and α-ω-dienes has a stronger influence on the elemental composition with decreasing chain length. Therefore, the differences in the H/C of the elemental analysis can be attributed to the significantly higher proportion of low-boiling HCs from pyrolysis in the ASR system. Consequently, the amount of compounds in the naphtha range obtained in the STR is lower for condensates of polyolefin-rich feedstocks.

5. Conclusion and outlook

This study provides a comprehensive overview of the feedstock influence and reactor-type dependent effects in the pyrolysis of thermoplastics at constant reactor temperature. The experimental investigations reveal their impact on the product yields and product compositions.

Ranging from 10.9 to 98.5 wt.%, the oil yields obtained in the STR system differ greatly for the pyrolyzed pure polymers. This emphasizes the decisive feedstock dependency in plastic pyrolysis. The product composition is highly polymer-dependent, covering a wide spectrum of organic HCs. Moreover, the reactor type affects the yields and compositions of the pyrolysis products. Enhanced gas formation by up to 22 wt.% is evident for all pure thermoplastics in the ASR system compared to the STR. The pyrolysis gases produced from LDPE and PP, as well as Mix A, seem suitable for use in the chemical industry after appropriate separation into ethene, propene, aromatics, or liquified petroleum gas. Pyrolyzing the more complex mixtures in the STR, high amounts of heteroatom-containing gas species of up to 27 wt.% are formed.

Varying results in different reactors can be attributed to characteristic reactor properties. Despite the preheated sand bed and rapid homogenization in the STR, temperature differences between the reactor wall and the polymer of 96 °C are measured at maximum. These differences are highly time-dependent, resulting from the semi-continuous dosing method. Despite the time-dependent polymer temperature profile, the GRT distribution of primary products is a decisive parameter. With 40 s, the minimum GRT in the heavier ASR reactor is twice as high as compared to the STR. The backmixing in the considerably larger freeboard of the ASR also leads to a GRT distribution width of about 5 min. The distribution width in the gas phase of the STR accounts for only 84 s. This promotes secondary cracking in the gas phase of the ASR, associated with the increased gas yields. In line with this, simulated distillation analyses indicate increased fractions of naphtha and middle distillate-like product cuts in the condensate by approximately 36 wt.% for the PCW. The increased gas formation in the ASR has no or only minor influence on the heteroatom content in the condensates measured within this study. In addition, the n- and iso-aliphatic compounds are predominantly unsaturated, which complicates the further use of the pyrolysis oils from both reactors. As the composition of the product fractions determines their suitability for chemical recycling, further purification and upgrading of the products before introducing them into petrochemical processes is required. Because of the strong influence of the reactor type on the product composition, this effort for subsequent processing can vary depending on the pyrolysis technology.

However, the reactor-type influence is less pronounced for Mix B, Mix C, or the PCW, as interaction effects occur in these complex mixtures that comprise heteroatom-containing polymers. Consequently, the interactions between polymers during pyrolytic decomposition seem to dominate the reactor-type-related effects. They prevent superposition-based estimations regarding product yields of heteroatom-containing mixtures under the experimental conditions. As a result of these interactions, the condensate yield is overestimated by 19–22 wt.%. Analyses of the product composition hint at the hypothesis that interactions intensify the cracking of polymer chains into lighter heteroatom-containing HCs during co-pyrolysis of PVC, PA6, PET, and ABS. This also leads to an overestimation of oxygen and nitrogen content in the condensate by superposition estimations for complex mixtures by up to 1.3 wt.%. Thus, the calculation approach is not suitable for the estimation of heteroatom impurities in the pyrolysis oil when applied to mixed plastics comprising heteroatom-containing polymers. In contrast, the superposition-based calculation is valid for determining the product yields and compositions for simple polymer mixtures, only including PE, PP, and PS. Estimations regarding the product yields or the elemental analysis of the condensate only deviate by a maximum of 0.6 and 0.4 wt.%, respectively.

However, reactor-specific variations can complicate a general and exact calculation of yields, boiling cuts, or product compositions during reactor scale-up. Heat and mass transfer limitations, along with the endothermic nature of pyrolysis, cause different results in the reactors even with identical feedstocks and reactor wall temperatures. Therefore, specifying the reactor type and the set temperature is only a superficial

assessment criterion for comparing pyrolysis results. Thus, further pyrolysis studies on a technical scale should provide a detailed reactor and process parameter characterization. Additional method development for measuring the polymer temperature profile in complex reactor geometries is required.

Moreover, detailed investigations of the pyrolysis behavior of complex plastic mixtures and an extension to other polymers are essential for understanding mechanisms of identified interaction effects and, thus, the complex pyrolysis mechanism. These studies must also concentrate on the GRT influence on the pyrolysis of mixed plastics.

CRediT authorship contribution statement

Harald Wehner: Investigation. **Dirk Eidam:** Writing – review & editing, Resources. **Orhan Keskin:** Investigation. **Britta Bergfeldt:** Writing – review & editing, Resources, Formal analysis. **Salar Tavakkol:** Writing – review & editing, Supervision, Resources, Funding acquisition. **Dieter Stapf:** Writing – review & editing, Supervision, Resources, Funding acquisition. **Niklas Netsch:** Writing – original draft, Visualization, Validation, Methodology, Investigation, Formal analysis, Data curation, Conceptualization. **Aljoscha Tauber:** Investigation, Data curation.

Funding

The study was funded by the German Helmholtz Association within the program „Materials and Technologies for the Energy Transition“.

Declaration of Competing Interest

The authors declare that they have no known competing financial interests or personal relationships that could have appeared to influence the work reported in this paper.

Acknowledgments

Technical support in the construction of the system was provided by Frank Richter, Sebastian Finger, Benjamin Seith, and Jens Jehle. The authors also gratefully acknowledge the assistance of Patrick Schieber, Galina Schuler, Michael Zeller, Grazyna Straczewski, Ankh-Erdene Erdenepurev, and Aylin Hannemann in supporting the pyrolysis gas and condensate analysis. Monika Schleinkofer and Julia Podszuweit performed the elemental analysis. The authors thank Feichi Zhang and Yufei Cao for their support with the technical drawing of the stirrer used in the stirred tank reactor.

Appendix A. Supporting information

Supplementary data associated with this article can be found in the online version at doi:10.1016/j.jaap.2025.107575.

Data availability

Data will be made available on request.

References

[1] R. Geyer, J.R. Jambeck, K.L. Law, Production, use, and fate of all plastics ever made, Sci. Adv. 3 (2017) e1700782, https://doi.org/10.1126/sciadv.1700782.
[2] F.D.B. de Sousa, The role of plastic concerning the sustainable development goals: The literature point of view, Clean. Respons. Consum. 3 (2021) 100020, https://doi.org/10.1016/j.clrc.2021.100020.
[3] I. Vollmer, M.J.F. Jenks, M.C.P. Roelands, R.J. White, T. van Harmelen, P. de Wild, G.P. van der Laan, F. Meirer, J.T.F. Keurentjes, B.M. Weckhuysen, Beyond mechanical recycling: giving new life to plastic waste, Angew. Chem. Int. Ed. 59 (2020) 15402–15423, https://doi.org/10.1002/anie.201915651.
[4] K.M. van Geem, Plastic waste recycling is gaining momentum, Science 381 (2023) 607–608, https://doi.org/10.1126/science.adj2807.
[5] A. Rahimi, J.M. García, Chemical recycling of waste plastics for new materials production, Nat. Rev. Chem. 1 (2017), https://doi.org/10.1038/s41570-017-0046.
[6] K. Ragaert, L. Delva, K. van Geem, Mechanical and chemical recycling of solid plastic waste, Waste Manag. 69 (2017) 24–58, https://doi.org/10.1016/j.wasman.2017.07.044.
[7] G. Lopez, M. Artetxe, M. Amutio, J. Bilbao, M. Olazar, Thermochemical routes for the valorization of waste polyolefinic plastics to produce fuels and chemicals. A review, Renew. Sustain. Energy Rev. 73 (2017) 346–368, https://doi.org/10.1016/j.rser.2017.01.142.
[8] T. Maqsood, J. Dai, Y. Zhang, M. Guang, B. Li, Pyrolysis of plastic species: A review of resources and products, J. Anal. Appl. Pyrolysis 159 (2021) 105295, https://doi.org/10.1016/j.jaap.2021.105295.
[9] V.K. Soni, G. Singh, B.K. Vijayan, A. Chopra, G.S. Kapur, S.S.V. Ramakumar, Thermochemical recycling of waste plastics by pyrolysis: a review, Energy Fuels 35 (2021) 12763–12808, https://doi.org/10.1021/acs.energyfuels.1c01292.
[10] P.T. Williams, E.A. Williams, Interaction of plastics in mixed-plastics pyrolysis, Energy Fuels 13 (1999) 188–196, https://doi.org/10.1021/ef980163x.
[11] N. Netsch, L. Schröder, M. Zeller, I. Neugber, D. Merz, C.O. Klein, S. Tavakkol, D. Stapf, Thermogravimetric study on thermal degradation kinetics and polymer interactions in mixed thermoplastics, J. Therm. Anal. Calor. 150 (2025) 211–229, https://doi.org/10.1007/s10973-024-13630-6.
[12] S.H. Chang, Plastic waste as pyrolysis feedstock for plastic oil production: A review, Sci. Total Environ. 877 (2023) 162719, https://doi.org/10.1016/j.scitotenv.2023.162719.
[13] M. Laghezza, S. Fiore, F. Berruti, A review on the pyrolytic conversion of plastic waste into fuels and chemicals, J. Anal. Appl. Pyrolysis (J. Anal. Appl. Pyrolysis) 179 (2024) 106479, https://doi.org/10.1016/j.jaap.2024.106479.
[14] F. Faisal, M.G. Rasul, M.I. Jahirul, D. Schaller, Pyrolytic conversion of waste plastics to energy products: A review on yields, properties, and production costs, Sci. Total Environ. 861 (2023) 160721, https://doi.org/10.1016/j.scitotenv.2022.160721.
[15] S. Honus, S. Kumagai, G. Fedorko, V. Molnár, T. Yoshioka, Pyrolysis gases produced from individual and mixed PE, PP, PS, PVC, and PET-Part I: production and physical properties, Fuel 221 (2018) 346–360, https://doi.org/10.1016/j.fuel.2018.02.074.
[16] V. Cozzani, C. Nicolella, M. Rovatti, L. Tognotti, Influence of gas-phase reactions on the product yields obtained in the pyrolysis of polyethylene, Ind. Eng. Chem. Res. 36 (1997) 342–348, https://doi.org/10.1021/ie950779z.
[17] A. López, I. de Marco, B.M. Caballero, M.F. Laresgoiti, A. Adrados, Influence of time and temperature on pyrolysis of plastic wastes in a semi-batch reactor, Chem. Eng. J. 173 (2011) 62–71, https://doi.org/10.1016/j.cej.2011.07.037.
[18] L. Dai, N. Zhou, Y. Lv, Y. Cheng, Y. Wang, Y. Liu, K. Cobb, P. Chen, H. Lei, R. Ruan, Pyrolysis technology for plastic waste recycling: a state-of-the-art review, Prog. Energy Combust. Sci. 93 (2022) 101021, https://doi.org/10.1016/j.pecs.2022.101021.
[19] N. Hassibi, Y. Quiring, V. Carré, F. Aubriet, L. Vernex-Loset, G. Mauviel, V. Burklé-Vitzthum, Analysis and control of products obtained from pyrolysis of polypropylene using a reflux semi-batch reactor and GC-MS/FID and FT-ICR MS, J. Anal. Appl. Pyrolysis 169 (2023) 105826, https://doi.org/10.1016/j.jaap.2022.105826.
[20] N. Hassibi, Y.A. Vega-Bustos, M.H. Aissaoui, G. Mauviel, V. Burklé-Vitzthum, Thermochemical Recycling of Polystyrene by Pyrolysis: Importance of the Reflux to Maximize the Production of Styrene and BTEX, Ind. Eng. Chem. Res. 62 (2023) 13432–13439, https://doi.org/10.1021/acs.iecr.3c01692.
[21] C. Stallkamp, M. Hennig, R. Volk, D. Stapf, F. Schultmann, Pyrolysis of mixed engineering plastics: Economic challenges for automotive plastic waste, Waste Manag. 176 (2024) 105–116, https://doi.org/10.1016/j.wasman.2024.01.035.
[22] H.C. Genuino, M.C.P. van Eijk, S.R.A. Kersten, M.P. Ruiz, Pyrolysis of real packaging plastic waste streams in a fluidized-bed pilot plant, Energy Fuels (2024), https://doi.org/10.1021/acs.energyfuels.3c04114.
[23] N. Netsch, M. Zeller, F. Richter, B. Bergfeldt, S. Tavakkol, D. Stapf, Energy Demand for Pyrolysis of Mixed Thermoplastics and Waste Plastics in Chemical Recycling: Model Prediction and Pilot-Scale Validation, ACS Sustain. Resour. Manag. 1 (2024) 1485–1492, https://doi.org/10.1021/acssusresmgt.4c00109.
[24] J.-J. Zhang, N. Ren, J.-H. Bai, Non-isothermal decomposition reaction kinetics of the magnesium oxalate dihydrate, Chin. J. Chem. 24 (2006) 360–364, https://doi.org/10.1002/cjoc.200690069.
[25] M. Calero, R.R. Solís, M.J. Muñoz-Batista, A. Pérez, G. Blázquez, M. Ángeles Martín-Lara, Oil and gas production from the pyrolytic transformation of recycled plastic waste: an integral study by polymer families, Chem. Eng. Sci. 271 (2023) 118569, https://doi.org/10.1016/j.ces.2023.118569.
[26] S.M. Al-Salem, A. Antelava, A. Constantinou, G. Manos, A. Dutta, A review on thermal and catalytic pyrolysis of plastic solid waste (PSW), J. Environ. Manag. 197 (2017) 177–198, https://doi.org/10.1016/j.jenvman.2017.03.084.
[27] M. Zeller, S. Tavakkol, D. Stapf, Experimental and analytical tools for the chemical recycling of engineering plastics - A multi-scale pyrolysis study on polydicyclopentadiene, Macromol. Rapid Commun. (2025) e2500161, https://doi.org/10.1002/marc.202500161.
[28] N. Netsch, L. Weigel, T. Schmedding, M. Zeller, B. Bergfeldt, G. Straczewski, S. Tavakkol, D. Stapf, Chemical characterization of mixed plastic pyrolysis oils relevant for cracker reintegration by advanced two-dimensional gas chromatography, Fuel Process. Tech. 280 (2025) 108359, https://doi.org/10.1016/j.fuproc.2025.108359.
[29] H.C. Genuino, M. Pilar Ruiz, H.J. Heeres, S.R.A. Kersten, Pyrolysis of mixed plastic waste: Predicting the product yields, Waste Manag. 156 (2023) 208–215, https://doi.org/10.1016/j.wasman.2022.11.040.

[30] T. Faravelli, M. Pinciroli, F. Pisano, G. Bozzano, M. Dente, E. Ranzi, Thermal degradation of polystyrene, J. Anal. Appl. Pyrolysis 60 (2001) 103–121, https://doi.org/10.1016/S0165-2370(00)00159-5.
[31] J. Yu, L. Sun, C. Ma, Y. Qiao, H. Yao, Thermal degradation of PVC: A review, Waste Manag. 48 (2016) 300–314, https://doi.org/10.1016/j.wasman.2015.11.041.
[32] H. Bockhorn, A. Hornung, U. Hornung, J. Weichmann, Kinetic study on the non-catalysed and catalysed degradation of polyamide 6 with isothermal and dynamic methods, Thermochim. Acta 337 (1999) 97–110, https://doi.org/10.1016/S0040-6031(99)00151-3.
[33] L. dos S. Vargette, H. Mohamadzadeh Shirazi, O. Mynko, M. Kusenberg, J. Jamieson, A.E. Muñoz Gandarillas, S. Ukkandath Aravindakshan, M.-F. Reyniers, K.M. van Geem, Comprehensive fouling assessment in steam crackers: fossil versus Renewable NEXBTL Naphtha, Ind. Eng. Chem. Res. 63 (2024) 111–120, https://doi.org/10.1021/acs.iecr.3c02969.
[34] M. Espinosa-Peña, Y. Figueroa-Gómez, F. Jiménez-Cruz, Simulated distillation yield curves in heavy crude oils: a comparison of precision between ASTM D-5307 and ASTM D-2892 physical distillation, Energy Fuels 18 (2004) 1832–1840, https://doi.org/10.1021/ef049919k.
[35] H. Bockhorn, A. Hornung, U. Hornung, D. Schawaller, Kinetic study on the thermal degradation of polypropylene and polyethylene, J. Anal. Appl. Pyrolysis 48 (1999) 93–109, https://doi.org/10.1016/S0165-2370(98)00131-4.
[36] K.-H. Lee, D.-H. Shin, Y.-H. Seo, Thermal degradation of nitrogen-containing polymers, acrylonitrile-butadiene-styrene and styrene-acrylonitrile, Korean J. Chem. Eng. 23 (2006) 224–229, https://doi.org/10.1007/BF02705720.
[37] C. Perego, R. Revel, O. Durupthy, S. Cassaignon, J.-P. Jolivet, Thermal stability of TiO2-anatase: Impact of nanoparticles morphology on kinetic phase transformation, Solid State Sci. 12 (2010) 989–995, https://doi.org/10.1016/j.solidstatesciences.2009.07.021.
[38] V. Georgieva, L. Vlaev, K. Gyurova, Non-Isothermal Degradation Kinetics of CaCO 3 from Different Origin, J. Chem. (2013), https://doi.org/10.1155/2013/872981.
[39] K. Paydar, A. Ebadi, A. Ahmadi, M. Manteghian, Investigation of the effect of temperature and grain size on the kinetic of hydrochloric acid and calcium carbonate reaction as a simulation of wellbore acidizing, J. Chem. Pet. Eng. (2023), https://doi.org/10.22059/jchpe.2023.357815.1429.
[40] M. Kusenberg, A. Eschenbacher, M.R. Djokic, A. Zayoud, K. Ragaert, S. de Meester, K.M. van Geem, Opportunities and challenges for the application of post-consumer plastic waste pyrolysis oils as steam cracker feedstocks: To decontaminate or not to decontaminate? Waste Manag. 138 (2022) 83–115, https://doi.org/10.1016/j.wasman.2021.11.009.
[41] R. Cao, M.-Q. Zhang, Y. Jiao, Y. Li, B. Sun, D. Xiao, M. Wang, D. Ma, Co-upcycling of polyvinyl chloride and polyesters, Nat. Sustain 6 (2023) 1685–1692, https://doi.org/10.1038/s41893-023-01234-1.